Magmatic processes at Snæfell volcano, Iceland, constrained by zircon ages, isotopes, and trace elements

Tenley J. Banik[1], Tamara L. Carley[2], Matthew A. Coble[3,7], John M. Hanchar[4], Justin P. Dodd[5], Gabriele M. Casale[6], Sean P. McGuire[1]

[1]Dept. of Geography, Geology, and the Environment, Illinois State University, Normal, IL 61790 USA; [2]Dept. of Geology and Environmental Geosciences, Lafayette College, Easton, PA 18042 USA; [3]Dept. Geological Sciences, Stanford University, Stanford, CA 94305 USA; [4]Dept. of Earth Sciences, Memorial University of Newfoundland, St. John's, NL A1B 3X5, Canada; [5]Dept. of Geology and Environmental Geosciences, Northern Illinois University, DeKalb, IL 60115 USA; [6]Dept. of Geological and Environmental Sciences, Appalachian State University, Boone, NC 28608 USA; [7]School of Geography, Environment and Earth Sciences, Victoria University of Wellington, Wellington 6140, New Zealand

Corresponding author: Tenley J. Banik (tjbanik@ilstu.edu)

Key Points:

- First zircon-based constraints on longevity and petrogenetic processes associated with production of rhyolites at Snæfell volcano, Iceland
- Zircon crystallization and residence occurs on timescales up to ~200 kyr at Snæfell—much longer than at other studied Neovolcanic centers
- Hf and O isotopes in zircon reveal petrogenesis dominated by fractional crystallization of mantle melts with minor crustal assimilation

Abstract

We present the first zircon-based U-Pb geochronology, trace element concentrations, and O and Hf isotope compositions for Snæfell, an off-rift volcano in eastern Iceland. These data provide constraints on the longevity and petrogenetic conditions of the Snæfell magmatic system. U-Pb zircon ages range from 545±59 to 266±16 ka (2SE), but differences between grain core and mantle ages within each sample reveal zircon residence times of 100–200 kyr—far longer than observed at other Neovolcanic systems in Iceland. Zircon $\delta^{18}O$ is restricted to ~3.5 to 4‰, and zircon ε_{Hf} ranges ~+13 to ~+17, which is substantially more radiogenic than Snæfell basalts. This combined O and Hf isotopic perspective suggests rhyolite petrogenesis at Snæfell can be attributed to fractional crystallization of mantle-derived basaltic magmas with limited influence of pre-existing crustal material. Trace element evidence further characterizes the magmatic source material: Sc/Yb <~0.01 suggests an amphibole-free petrogenetic environment, and Ti concentrations in zircon <5 ppm suggest a cool, near-solidus, crystallization environment for the majority of the zircon's pre-eruptive history, with elevated Ti in zircon surfaces suggesting a late thermal perturbation, perhaps a mafic input that remobilized (to the point of eruption triggering) near-solidus magmas. These zircon-based conclusions are broadly consistent with previous interpretations of rhyolite petrogenesis conditions at Snæfell but provide a multi-faceted perspective with more detailed resolution of source materials, magma generating processes, system longevity, and pre-eruptive conditions.

1 Introduction

Silicic (≥65 wt% SiO_2) magma petrogenesis in Iceland is enigmatic and the subject of ongoing study. Proposed mechanisms of magma production invoke partial melting of the hydrothermally altered, dominantly (>~90%) basaltic crust (e.g., Óskarsson et al., 1982; Marsh et al., 1991; Sigmarsson et al., 1991; Jónasson, 1994; Gunnarsson et al., 1998; Bindeman et al., 2012), fractional crystallization (FC) of primary basaltic magma (e.g., Carmichael, 1964; Macdonald et al., 1987; Nicholson et al., 1991; Furman et al., 1992; Prestvik et al., 2001; McGarvie, 2009), and both processes, either independently or acting in tandem (e.g., Sigmarsson et al., 1992a, b; Martin & Sigmarsson, 2010). Tectonic location (on-rift vs. off-rift) is often cited as a major factor in determining which of these processes dominates silicic petrogenesis at different systems in Iceland (Figure 1); partial melting of hydrothermally altered crust is often invoked as the dominant process in hotter, on-rift systems, while fractional crystallization is proposed to dominate in cooler, off-rift systems (e.g., Jónasson et al., 1992; Jónasson, 2007; Martin & Sigmarsson, 2007; Schattel et al., 2014). Recent whole rock and zircon isotopic studies suggest that other factors, such as age of the rift, age and composition of the underlying bedrock, and thermal priming of the crust all play crucial roles in ultimately producing silicic magmas (e.g., Banik et al., 2018; Carley et al., 2020). Uncertainty regarding the degree to which anatectic melts, melts derived from primary basalt fractionation, or melts from assimilation and fractional crystallization (AFC) processes contribute to silicic magmas persists in part due to the complicated assembly and geochemistry of the Icelandic crust (e.g., Darbyshire et al., 2000; Hardarson & Fitton, 1997; Martin et al., 2011) and the chemically heterogeneous nature of the underlying mantle (e.g., Hanan & Schilling, 1997; Kitagawa et al., 2008; Kokfelt et al., 2006; Peate et al., 2010; Prestvik et al., 2001; Thirlwall et al., 2004). Investigation of silicic

petrogenesis commonly focusses on Neovolcanic (<0.78 Ma) systems because they are numerous and have less-eroded outcrops relative to older systems; on-rift systems are better-understood than off-rift systems because they are associated with better-constrained underlying crustal structures, minimizing some of the uncertainty described above.

Of particular interest is the production of silicic magmas in off-rift, or flank, zones, since these areas are poorly understood relative to the settings on-rift Neovolcanic central volcanoes (Figure 1). Off-rift volcanism in Iceland comprises the Snæfellsnes volcanic belt (SVB) in the west and the Öræfi volcanic belt (ÖVB) in the southeast (Figure 1a). Snæfell, the focus of this study, defines the northern end of the ÖVB. In the SVB, magmatism is hypothesized to result from a thermal pulse from the Iceland mantle plume acting on the thin crust along the previously active rift axis (e.g., Walters et al., 2013). ÖVB magmatism is less clear. The ÖVB may represent an incipient rift that parallels and will eventually take over from the currently active Northern and Eastern rifts (e.g., Walker, 1975) (Figure 1b). It is hypothesized that remnant continental crust segments from earlier North Atlantic rifting may be trapped under eastern Iceland (Foulger, 2006; Martin et al., 2011; Torsvik et al., 2015), contributing to magmas with distinct geochemical characteristics (e.g., Hards et al., 2000; Prestvik et al., 2001; Peate et al., 2010).

Figure 1. (a) Iceland bedrock ages. Numbers 1 (Snæfellsnes) and 2 (Öræfi) are off-rift volcanic belts. Modified from Harðarson et al., 2008. (b) Relief map of southeastern Iceland and the Öræfi volcanic belt. Dashed line separates Neovolcanic (<0.78 Ma) and older bedrock. Low relief coastal areas immediately surrounding Öræfajökull and the southern and eastern margins of Vatnajökull are composed of Holocene sandur deposits. (c) General geologic map of the Snæfell volcanic system and surroundings overlain on regional DEM; grey background is mafic/int. extrusive rocks and sediments of Lower Pleistocene age (0.8–2.6 Ma). Geology based on a system maps

from Hards, 1995 and the 1:600,000 Iceland map of Hjartarson & Sæmundsson, 2014. DEMs from Landmælingar Íslands (lmi.is).

One of the issues that is not widely well-quantified in Icelandic systems—and is perhaps volcano-specific—is the residence time associated with silicic magmas and the processes responsible for their eruption. Understanding residence time is important because longevity and destabilization are fundamentally linked to petrogenesis writ large (e.g., Halliday et al., 1989; Gardner et al., 2002; Schmitt et al., 2003; Zellmer et al., 2005; Folkes et al., 2011; Reid et al., 2011). Whole rock geochemical analyses from active and extinct volcanic systems across Iceland are abundant and discussion of certain aspects of magma evolution, such as phase equilibria and liquid lines of descent, are much-utilized tools in investigation of petrogenesis (e.g., Óskarsson et al., 1982; Sigmarsson et al., 1992b; Mattsson & Oskarsson, 2005; Kitagawa et al., 2008; Peate et al., 2010; Martin et al., 2011; Manning & Thirlwall, 2014). More recently, U-series isotopic data have provided constraints on magma differentiation and residence that suggest timescales on the order of 10s of kyr or less for both on-rift and off-rift systems. Sigmarsson (1996) reports FC of alkali basalt to hawaiite and mugearite requires only a 10-year residence in the Vestmannaeyjar. Krafla basalts are hypothesized to spend <9 ka in the crust prior to eruption (Cooper et al., 2016). AFC models for Hekla (on-rift) suggest that FC of basalt to produce basaltic andesite occurs on a timescale of ~20 kyr, while assimilation of crustal material and FC of basaltic andesite produces andesite in only ~2 kyr (Chekol et al., 2011). Studies that incorporate silicic magmas suggest understandably longer timescales: rhyolites at Torfajökull (on-rift) appear to have been generated via anatexis in <~10 kyr (Zellmer et al., 2008). At off-rift Snæfellsjökull, U-series data suggest derivation of hawaiite from olivine basalt within ~12 kyr and trachyte within ~54 kyr from closed system FC processes. These types of analyses provide critical constraints on near-

continuously active magmatic processes; however, prior zircon-based studies suggest that silicic magmas in Iceland likely spend significant portions of their lifetimes in near-solidus to sub-solidus conditions prior to being rejuvenated or erupted (Carley et al., 2011, 2014, 2017, 2020; Padilla et al., 2016; Banik et al., 2018; cf. Martin et al., 2011).

Zircon is an important mineralogical tool in studies of intermediate and silicic magma residence time, longevity, source region(s), and intra-magma body processes (e.g., Reid et al., 1997; Charlier et al., 2005; Bachmann et al., 2007; Folkes et al., 2011; Reid et al., 2011; Stelten & Cooper, 2012). In many instances, zircon is also the most reliable repository of elemental and isotopic conditions in the host magma due to its chemical and physical durability and slow volume diffusion rates when crystalline (i.e., not metamict) (e.g., Cherniak & Watson, 2003; Finch & Hanchar, 2003).

The only published petrogenetic study focused on the Snæfell volcanic system (Figure 1c) uses whole-rock analyses to propose a petrogenetic model in which magmas are largely juvenile; rhyolites evolve via fractional crystallization of basaltic mantle melts at ~10–15 km depth with minor contamination by pre-existing crust (Hards et al., 2000). Those authors hint at the presence of long-lived, stratified magma bodies in a zone of immature rifting as the source for Snæfell magmas. However, structural evidence is lacking for a close relationship between volcanism and rifting at Snæfell—the only connection is the linear relationship along the ÖVB volcanic centers (cf. Thordarson & Höskuldsson, 2014) (Figure 1b).

In the present study, we combine U–Pb ages from zircon interiors and unpolished surfaces to assess zircon growth timescales with trace elemental compositions to assess temporal changes in magmatic conditions at Snæfell. This temporal perspective may reflect changes in magma storage and evolution at depth. High spatial resolution isotope compositions in zircon (Hf

and O) further contextualize their source magmas and provide insights for which model(s) best explain Snæfell silicic magma petrogenesis. These multiple lines of evidence provide a more detailed view into silicic magma genesis at Snæfell (with potential implications for other off-rift systems) and demonstrate the utility of zircon geochronology, trace elements, and Hf and O isotope compositions for assessing magmatic source materials and residence times and conditions.

2 Geologic Setting and Background

Snæfell central volcano occupies the northern end of the off-rift Öræfi Volcanic Belt (ÖVB) in eastern Iceland (Figure 1). It is the tallest subaerial volcano in Iceland at 1833 m (Sæmundsson, 1979), although the vast majority of its eruptive products were emplaced under ice cover (e.g., Helgason et al., 2005). In addition to the main edifice, the Snæfell system comprises a series of fissures and smaller subglacial eruptive features, all of which are oriented roughly parallel to the currently active Northern rift zone trending approximately 027° (Figure 1).

As is common in Icelandic central volcanoes, Snæfell magmatism is bimodal, with dominant basalt, subordinate rhyolite, and minimal intermediate composition magmas. Rhyolites occur as effusive domes and plugs and have experienced a shallow level of erosion (Hards et al., 2000). Snæfell magmas are part of the transitional alkalic series, which is common amongst the vast majority of off-rift volcanic centers in Iceland (e.g., Jakobsson et al., 2008). Transitional alkalic magma compositions such as these tend to have higher TiO_2 and FeO for a given MgO content and more restricted MgO overall. Nepheline-normative basalts are part of the transitional alkalic series at Snæfell; rhyolites are peralkaline. Both rock types are commonly phenocryst-

poor, but occasionally display glomerocrysts of olivine, plagioclase, and augite; rhyolites have accessory apatite and zircon (Hards et al., 2000). The reader is referred to Hards et al. (2000) and Höskuldsson and Imsland (1998) for excellent summaries of the volcano geology and eruptive products of Snæfell.

Snæfell unconformably overlies basaltic bedrock of Plio-Pleistocene age, although some authors posit that the bedrock may have formed around 10 Ma (Ivarsson, 1992; Martin et al., 2011). Helgason et al. (2005) report ^{40}Ar–^{39}Ar ages of 256±28 ka (2σ) for a basaltic unit at Snæfell's summit and 466±40 ka for a basal trachyandesite. These authors also determined an age of 1.35±28 Ma (2σ) for a basalt that lies stratigraphically under Snæfell (Helgason et al., 2005). Additional basalt flows at the base of Snæfell have K–Ar ages of 255±8, 274±8, and 324±12 (2σ) ka (Guillou et al., 2010). Guillou et al. (2010) also report a rhyolite near the summit of Snæfell with a K–Ar age of 253±6 (2σ) ka that has been subsequently refined via ^{40}Ar–^{39}Ar dating to 207±10 (2σ) ka (Guillou et al., 2019). These ages suggest that the main stage of edifice building lasted from ~466 to 200 ka. Additional units considered part of the Snæfell volcanic system but not part of the main edifice have been dated at 400±47 ka (basalt) and 310±50 ka (rhyolite) (Höskuldsson et al., 1996). Notably absent for Snæfell are zircon crystallization ages that can provide information on timescales of magmatic processes or longevity of silicic magmas prior to eruption or edifice construction.

3 Methods

Whole rock samples (*n*=3*)* were collected from Snæfell rhyolite units in consultation with the geologic map of Hards (1995) (Table 1). Fresh slices of rock, with weathered or otherwise visibly altered materials removed, were prepared and reserved for whole rock geochemical

177 analysis. Zircon was separated from the remaining sample material via standard crushing,
178 sieving, and conventional magnetic and density separation methods, followed by hand-picking
179 with a binocular microscope. Zircon in Snæfell samples is relatively abundant for Icelandic
180 rhyolites (~100–200 grains/kg). A subset of euhedral grains was pressed into an indium mount
181 and imaged via reflected light microscopy prior to surface analysis. Remaining zircon grains
182 were cast in epoxy and polished to expose the grain interiors. Prior to analysis, polished grains
183 were imaged using CL and BSE with a Tescan VEGA3 scanning electron microscope at
184 Vanderbilt University and a JEOL JSM-IT-300LV scanning electron microscope equipped with
185 a Gatan ChromaCL2 in the Dewel Microscopy Facility at Appalachian State University (Figure 2
186 and Supplemental Figure S1).

187 **Table 1.** Sample locations, descriptions, and bulk rock oxygen isotope analyses.

188 **Figure 2.** Cathodoluminescence (CL) images of representative Snæfell zircon grains. Grains A–B=sample IESn1;
189 C–I =sample IESn2; J–L=sample IESn3. Grains C, D, and K display penetration twinning seen in all sampled
190 locations. Grain I has a distinct, oscillatory-zoned euhedral core and an unzoned mantle, while grain C shows faint
191 oscillatory zoning. Faint sector zoning in visible in grains B, H, and J; L has distinct sector zoning. A CL-bright core
192 with a dark mantle is clearly visible in Grain K. Most grains have a faint overgrowth rim. Maximum CL intensity is
193 the same in grains A–I; J–L are color CL.

194 Zircon grains from all three samples (IESn1, IESn2, and IESn3) were analyzed for trace
195 elements and U-Pb geochronology. After a light polish, O isotope compositions were measured,
196 followed by Hf isotopes. Care was taken to avoid analyzing O isotopes within ~5 μm of any
197 previous analytical spot. Zircon U–Pb ages and trace element compositions were obtained using
198 the sensitive high-resolution ion microprobe with reverse geometry (SHRIMP-RG) jointly
199 operated by the U.S. Geological Survey and Stanford University. We selected grain interiors

based on the common textural observation of potentially ante- or xenocrystic cores that are visible in CL for a subset of grains in each sample (Figure 2). Operating procedure included an O_2^- primary ion beam focused to a ~14x18 μm diameter spot for trace element analyses and a ~30x40 μm diameter spot for U–Pb isotopes (Supplemental Tables S1 and S2). Zircon U–Pb analyses were calibrated using zircon standard Temora-2 ($^{206}Pb/^{238}U$ age=416.8 Ma; Black et al., 2004) and trace element concentrations standardized relative to MAD-559 (Coble et al., 2018). Data were reduced using Squid 2.51 (Ludwig, 2009) and Isoplot 3.76 software (Ludwig, 2012). Measured $^{206}Pb/^{238}U$ was corrected for common Pb (Pb_c) using measured ^{207}Pb based on a model Pb composition from Stacey and Kramers (1975) and corrected for ^{230}Th disequilibrium using the method of Schärer (1984) and an initial assumed $(^{230}Th/^{238}U)_{melt}$ value based on whole rock Th/U values (Th/U=4.7 for IESn1 and IESn2; Th/U=3.7 for IESn3 based on values from the same units sampled by Hards (1995). The magnitude of the correction was typically 85–90 kyr.

We performed a total of 31 O isotope analyses on zircon crystals from all three samples (IESn1, IESn2, and IESn3) at the University of Wisconsin–Madison using a CAMECA ims-1280 secondary ion mass spectrometer (SIMS) following the method of Kita et al., (2009). Operating conditions include a Cs^+ primary ion beam with an analytical spot size of ~10 μm. Measured ratios were corrected for mass discrimination using primary zircon standard KIM-5 ($\delta^{18}O$=5.09±0.12‰ (2SD); Valley et al., 1998). Internal 2σ reproducibility for KIM-5 analyses ranged from 0.15 to 0.24‰ (see Supplemental Table S4). For comparison to zircon, whole rock O isotope compositions were measured via laser fluorination at the Stable Isotope Laboratory at Northern Illinois University according to the method of Sharp (1990). Fresh samples were crushed, sonicated in deionized water to remove residual powder, and sieved at > 250 μm size fraction. Typically, 1 to 2 mg of representative whole rock samples were then melted under

vacuum with a PhotonMachines Fusions 10.6 CO_2 laser in the presence of 10 kPa of BrF_5. O_2 gas generated by this reaction was isolated cryogenically by adsorption on a zeolite trap and transferred to a Thermo Finnigan MAT 253 isotope ratio mass spectrometer. Calculated O_2 yields were better than 95% for all samples. International and internal standards NBS-28 (9.6 ± 0.07‰, 2SD), UWG-2 (5.8 ± 0.10‰, 2SD), NIU Qtz (18.2 ± 0.10‰, 2SD), and EP43-75 (18.4 ± 0.20‰, 2SD) were analyzed with each sample run. All O isotope data are reported as $\delta^{18}O$ calculated relative to VSMOW of Baertschi (1976).

Zircon Lu–Hf isotope composition was measured on a subset of the same grains using laser ablation multi-collector inductively coupled plasma mass spectrometry (LA-MC-ICPMS) at Memorial University of Newfoundland. Grains subjected to previous analysis were prioritized for Hf isotope analysis, followed by grains that were large enough to accommodate the analytical spot. Sixty grains in total were analyzed for Lu–Hf isotope compositions using a ThermoFinnigan Neptune MC-ICP-MS coupled to a Geolas Pro 193 nm Ar-F excimer laser with an analytical spot diameter of ~40 μm, a 10 Hz repetition rate, and fluence of ~5 J/cm^3. We follow the instrument configuration, operating parameters, and data reduction methods outlined by Fisher et al. (2014), with the exception that U-Pb ages were not simultaneously determined. Secondary zircon standards used in this study covered the range of (Lu+Yb)/Hf of the samples studied. Primary zircon standards, determined by solution MC-ICP-MS (2SD uncertainty listed), were Plešovice ($^{176}Hf/^{177}Hf$=0.282482±13; Sláma et al., 2008), B142, and B144 ($^{176}Hf/^{177}Hf$=0.282140±5; Fisher et al., 2011). FC1 ($^{176}Hf/^{177}Hf$=0.282182±14; Vervoort, 2010); and R33 ($^{176}Hf/^{177}Hf$=0.282767±18; Vervoort, 2010) were analyzed as secondary standards. All standards were interspersed with unknowns to assess accuracy and external reproducibility. Laser ablation MC-ICPMS analyses of standard zircon grains yielded mean values for

246 $^{176}Hf/^{177}Hf$ as follows: Plešovice $^{176}Hf/^{177}Hf$=0.282481±7 (2SD; n=12); FC1
247 $^{176}Hf/^{177}Hf$=0.282177±9 (2SD; n=14); and R33 $^{176}Hf/^{177}Hf$=0.282762±5 (2SD; n=8). Analyses of
248 these secondary zircon standards agree well with published solution-MC-ICPMS determination
249 of the isotope composition of purified Hf from these zircon samples. Present day ε_{Hf} values were
250 calculated using the CHUR parameters reported by Bouvier et al. (2008). Use of present day ε_{Hf}
251 is standard for reporting such measurements in Icelandic materials due to their young (<15 Ma)
252 ages (e.g., Kitagawa et al., 2008). Laser Lu-Hf isotopic data are reported with 2σ uncertainty in
253 Table 2 and Supplemental Table S3.

254 Outliers >2 standard deviations from the mean were not incorporated into the reported
255 weighted means for sample age, $\delta^{18}O$, or ε_{Hf} values (Table 2, Figure 3).

256 **4 Results**

257 4.1 Characterization of zoning and crystal morphology

258 Separated Snæfell grains have maximum dimensions up to ~200 μm in length, with most
259 grains ~100 μm maximum length—a size range fairly typical for Icelandic volcanic zircon (e.g.,
260 Banik et al., 2018; Carley et al., 2011; Padilla et al., 2016). Snæfell zircon crystals are invariably
261 euhedral and typically have a ~2:1 aspect ratio. Grain habits are dominated by {101} and {100}
262 forms. Internal morphology is broadly consistent across samples, with several common
263 variations (Figure 2; Supplemental Figure S1). Most crystals display minimal CL intensity
264 variation within and between samples, although CL-bright, c-axis-parallel features commonly
265 occur in all samples. Igneous (e.g., oscillatory, sector) zoning is common. Many zircons display
266 clear internal boundaries that truncate existing zoning patterns. Roughly 10% of imaged grains in
267 IESn1 and IESn3 and ~20% of grains in IESn2 display a texture akin to twinning.

268 4.2 Zircon geochronology

269 Weighted mean sample ages for zircon cores are 443±36 ka (IESn1; *n*=3; 2SE), 545±59
270 ka (IESn2; *n*=7; 2SE), and 360±110 ka (IESn3; *n*=3; 2SE) (Table 2; Figure 3). Weighted mean
271 sample ages for mantles of grains and non-CL-discernable interiors are 353±13 ka (IESn1; *n*=13;
272 2SE), 356±12 ka (IESn2; *n*=20; 2SE), and 266±16 ka (IESn3; *n*=15; 2SE). One grain from
273 sample IESn1 is significantly older with an age of 1,075±584 ka (2SE). Surface age analyses
274 from sample IESn2 (*n*=2) are 441±131 ka and 344±39 ka, and 640±209 ka, 340±134 ka, and
275 297±144 ka from sample IESn3 (*n*=3). The range of values for mean squared weighted
276 deviations (MSWD; weighted by $1/\sigma^2$) for calculated weighted mean ages is 0.028–1.8. We
277 interpret MSWD values that are higher than would be expected for a homogeneous population
278 with a given *n* value (e.g., Mahon, 1996) to result from inheritance and represent an older zircon
279 crystallization history recorded in Snæfell magmas.

280 4.3 Zircon trace element concentrations

281 Approximately 100 trace element analyses were conducted on zircon interiors (*n*=76) and
282 surfaces (*n*=21). Titanium concentrations range from ~0–15 ppm (Figure 4; Supplemental Table
283 S2), and Ti concentrations in zircon surfaces of samples IESn2 and IESn3 are ~5 ppm higher
284 (sample means) than in grain interiors. Hafnium ranges from ~7,000–12,000 ppm, but only
285 sample IESn1 zircon has >10,500 ppm Hf. Zircon from sample IESn3 occupies a more restricted
286 range of Hf (7,000–8,000 ppm, with two outliers at ~9,000 and 9,500 ppm) than the other two
287 samples. Uranium and Th for sample IESn1 and IESn2 zircons are (~80–700 ppm and ~30–600
288 ppm, respectively) and Th/U ranges from 0.28 to 1.06, with most grains having Th/U between
289 0.25 and 0.75 (median=0.51; mean=0.53). Uranium and Th concentrations in zircon from sample

IESn3 range from ~100–700 ppm and ~40–750 ppm, respectively, with Th/U ranging from 0.44 to 1.07. Unlike sample IESn2 zircons, which have the same Th/U values in both zircon interiors and surfaces, IESn3 zircon interiors have higher mean (Th/U=0.71) and median (Th/U=0.66) Th/U values than zircon rims from the same sample (mean=0.56; median=0.57). Niobium concentrations range from ~10–250 ppm (Figure 4). Snæfell zircon has Sc concentrations that range from ~1 to 40 ppm, with a distinct sub-population of grains from samples IESn1 and IESn2 having Sc>10 ppm and Sc/Yb >0.02 ppm. Zircon from sample IESn3 has consistently low Sc (~1–5 ppm) and Sc/Yb (~0.0005–0.005). Snæfell zircon is enriched in heavy rare earth elements (HREE) relative to light rare earth elements (LREE) and displays positive Ce and negative Eu anomalies characteristic of magmatic zircon (Figure 5) when normalized to chondrite (McDonough & Sun, 1995). Zircon from sample IESn3 is more enriched in overall REE than zircon from the other samples; however, all Snæfell zircon analyses have the same general REE trend characteristic of Icelandic zircon from silicic magmas (Carley et al., 2014; Banik et al., 2018). There is no observable distinction in trace element trends between older grain cores and younger grain mantles.

4.4 Zircon oxygen isotope values

Oxygen isotope ratios ($\delta^{18}O_{VSMOW}$) for Snæfell zircon (*n*=31*)* range from ~3.08‰ to ~4.36‰ (Figure 3; Table 2). Zircon grains from IESn1 have $\delta^{18}O$ ranging from 3.56±0.20‰ to 4.12±0.24‰ (uncertainties are 2SE) with a weighted mean of 3.85±0.10‰ (MSWD = 1.9). Zircon grains from IESn2 have $\delta^{18}O$ from 3.08±0.24‰ to 3.80±0.25‰ with a weighted mean of 3.57±0.11‰ (MSWD=1.7). Oxygen isotope ratios for IESn3 zircon grains range from 3.55±0.21‰ to 4.36±0.38‰ with a weighted average of 3.73±0.11‰ (MSWD = 2.1).

Figure 3. Zircon analyses from Snæfell samples. Each vertical bar is a single analysis shown as ±2SE; open vertical bars are analyses not included in the weighted mean; horizontal boxes denote weighted sample means±2SE; thick black horizontal lines denote weighted sample means. Weighted sample means±2SE listed for each sample. (a) U-Pb ages. Ages are corrected for $^{207}Pb_c$ and ^{230}Th disequilibrium. Surface analyses are demarcated by the hatched pattern. (b) Oxygen isotope values. Grey field is average mantle zircon value from Valley et al. (1998). Corresponding whole rock $\delta^{18}O$ is white bar with 2σ uncertainty in black field. (c) ε_{Hf} values.

Figure 4. Selected trace element concentrations and variations in Snæfell zircon plotted against other Icelandic zircon (Banik et al., 2018; Carley et al., 2014). Open circles denote grain surface analyses; closed circles are grain interior analyses. (a) Ti vs. Hf. (b) Ti vs. Sc/Yb. (c) Ti vs. Yb. (d) Sc vs. Sc/Yb. Fractionation trends from Grimes et al. (2015).

Figure 5. Snæfell zircon (lines) vs. Icelandic zircon (grey field; Carley et al., 2014) REE, normalized to chondrite values of McDonough and Sun (1995).

Table 2. Summary of zircon isotope analyses. Ages are $^{207}Pb_c$- and ^{230}Th-corrected. Values in italics are not included in the sample mean.

4.5 Zircon hafnium isotope values

Hafnium isotope compositions were obtained for 60 Snæfell zircon grains (Figure 3, Table 2). The ε_{Hf} for Snæfell samples ranges from +13.3 to +17.8, which includes some of the highest individual ε_{Hf} values observed in Icelandic zircon (e.g., Carley et al., 2020). Samples IESn1and IESn2, which have nearly identical U-Pb ages and were collected in close proximity to one another, have weighted sample mean ε_{Hf} of +14.1±0.3 (2SE; MSWD=2.3) and +14.2±0.2

(MWSD=1.3), respectively. Younger sample IESn3 has a weighted sample mean ε_{Hf} of +14.7±0.4 (MSWD=2.2) and is the only sample to have individual grains with ε_{Hf} near or greater than ~+16.

4.6 Whole rock oxygen isotope values

Snæfell whole rock samples IESn1, IESn2, and IESn3 have $\delta^{18}O_{VSMOW}$ of 5.08±0.14‰ (n=3), 5.45±0.78‰ (n=3), and 5.43±0.42‰ (n=5), respectively (Figure 3; Table 1). Errors are 2SD. These data are consistent with previously published values of Snæfell whole rock rhyolites (~4.4–5.3‰; Hards et al., 2000). Relatively large uncertainties associated with samples IESn2 and IESn3 are attributed to visible sample heterogeneities characteristic of those outcrops and of the pieces analyzed.

5 Discussion

The results above provide a largely zircon-focused context (with supporting whole rock data) from which to interpret petrogenesis of rhyolites from Snæfell, including timing and longevity of the magmatic system, magmatic processes, and constraints on involvement of mantle vs. crustal materials.

5.1 Zircon crystallization timescales

Zircon geochronology expands our understanding of magmatic-volcanic timescales operating at Snæfell. The previously reported rhyolite age from the main edifice of Snæfell is 207±10 (2σ) ka (Guillou et al., 2019), which is younger than all the U-Pb zircon dates measured in this study . Samples IESn1 and IESn2 have weighted mean ages older than the oldest reported

basalt age (324±12 (2σ) ka; Guillou et al., 2010). We interpret the youngest population of zircon ages (weighted mean sample ages: IESn1: 353±13 ka; IESn2: 356±12 ka; and IESn3: 266±16 ka) from the interior analyses to represent maximum estimates of the eruption age. This is supported by the surface ages, despite their larger uncertainties due to high common Pb concentrations and relatively low U concentrations (Table 2). We interpret the older ages from zircon cores to arise from recycling of antecrystic zircon native to the Snæfell system—it is unlikely that the older zircon grains are truly xenocrystic due to the large discrepancy between zircon ages and the apparent bedrock ages (~2–10 Ma, increasing with depth). Mussett et al. (1980) report a basalt bedrock age of ~2.5 Ma ~20 km due northeast from the summit of Snæfell along the regional fissure orientation, which is likely a good estimate of the general shallow bedrock age immediately underlying Snæfell when the regional stratigraphy is considered. Combining Snæfell's distance from the eastern 3.3 Ma isochron on the geologic map of Iceland (Jóhannesson & Sæmundsson, 2009) and the current average spreading rate of ~1 cm/yr (DeMets et al., 2010) yields an model bedrock age of ~1.8 Ma, which increases to ~2.1 Ma using the 0.78 cm/yr spreading rate of Mussett et al. (1980). Although inconsistent spreading rates over the length of the rift (e.g., Walker, 1964, 1974; and many others) lead to uncertainty, this calculation nevertheless provides a rough approximation by which to assess potential bedrock age.

Intra-grain U-Pb measurements reveal timescales of magma residence previously unrecognized at Snæfell. Uranium-Pb analysis on a subset of ante- or xenocrystic-appearing cores (Miller et al., 2007) identified by CL imaging confirms that they are statistically older than the younger population of grains and grain mantles in each sample. These results suggest that many of the grains in samples IESn1 and IESn2 experienced an initial period of growth followed by residence in sub-solidus or zircon-undersaturated conditions—a common phenomenon in

zircon-bearing systems globally (e.g., Reid et al., 1997; Lowenstern et al., 2000; Schmitt et al., 2003; Miller & Wooden, 2004; Bacon & Lowenstern, 2005; Simon & Reid, 2005; Charlier et al., 2005; Claiborne et al., 2010).

In Iceland, zircon residence timescales prior to eruption approach 50 kyr in historically active systems (Carley et al., 2011), and apparently far longer in Tertiary systems (Carley et al., 2017; Banik et al., 2018). This apparent discrepancy in residence times between young and old systems may simply result from sampling bias: Tertiary systems are extinct and sampling has the potential to intersect grains from the entire zircon-saturated lifespan of the system, whereas currently active systems may not have erupted a sufficient volume, or been sufficiently dissected by erosion, to provide the 4-D sampling resolution possible for >1 Myr-old extinct systems. U-Th disequilibrium ages indicate zircon residence at Öræfajökull, located at the southern end of the ÖVB, was ~35 kyr for zircons erupted in 1362 CE. Hekla zircon residence is >40 kyr and Torfajökull zircon residence approaches ~50 kyr (Carley et al., 2011). Zircon crystallization, sub-solidus storage, and remobilization on timescales up to ~200 kyr appears to have been common at Snæfell, especially earlier in its magmatic history (Figure 3). This protracted zircon residence timescale is similar to that observed in arc volcanoes; for example, Mount St. Helens zircons have core-to-rim age variations up to 200 kyr and cores that are easily distinguishable in CL (Claiborne et al., 2010). This may imply that—similar to arc systems—Snæfell's plumbing structure allows for development of a long-lived 'rigid sponge' (Hildreth, 2004) formed through repeated melt injections, cooling and AFC processes, and rejuvenation. Snæfell zircon grains likely crystallized from multiple iterations of melts and were then amalgamated into their final host magma after varying degrees of residence time—a scenario supported by the variety of ages observed within these grains (Figure 3) and the commonly observed zonation patterns (Figure 2).

5.2 Thermal conditions of Snæfell rhyolites

Surface analyses of Snæfell zircon average ~5 ppm higher Ti than those observed in grain interiors (Figure 4); application of the Ti-in-zircon thermometer of Ferry and Watson (2007) with a_{SiO2}=1 and a_{TiO2}=0.5 yields surface crystallization temperatures ~50°C higher than grain interiors in samples IESn2 and IESn3 (Supplemental Table S6). Titanium concentrations in zircon correlate with crystallization temperature (Watson et al., 2006; Ferry & Watson, 2007). These findings suggest that the final crystallization interval of these zircon grains occurred in an environment that was substantially warmer than earlier stages of crystallization—likely from open-system processes involving the influence of new, hotter magma from the deep crust or mantle. Rejuvenation of crystal mushes through underplating or introduction of hotter material is a common and well-studied phenomenon (e.g. Mahood, 1990; Bachmann et al., 2002; Bachmann & Bergantz, 2009; Klemetti & Clynne, 2014).

In Iceland, the vast majority of magmatic systems with a central volcano (a main edifice) also have fissure systems that are capable of transporting magma sourced from depth. The general model for central volcano systems also includes a longer-lived, shallow reservoir that ultimately feeds central volcanoes (e.g., Walker, 1966; Thordarson & Larsen, 2007). A typical on-rift central volcano system in Iceland commonly appears to have a magma chamber at <5 km depth fed by dikes and/or magma reservoirs near the base of the crust (e.g. Gudmundsson & Högnadóttir, 2007; Maclennan, 2019; Thordarson & Larsen, 2007). Comparisons of phase equilibria and experiments support the presence of a mid-crustal magma reservoir under Snæfell at ~13 km depth (0.35 GPa; Hards et al., 2000), hosted in dominantly basaltic crust under Snæfell ~35 km thick (Darbyshire et al., 2000).

Snæfell was ~60 km from the currently active Northern rift axis during edifice construction, assuming an average half-spreading rate of ~1 cm/yr (DeMets et al., 2010). The subsurface model of Pálmason (1986) based on structural observations, geodetic measurements, and thermal modeling suggests bedrock temperatures corresponding to a 13 km-deep magma reservoir at Snæfell approach 900ºC—potentially too cold to initiate partial melting of the hydrated metabasaltic crust (modelled to begin ~1000ºC; Pálmason, 1986; cf. Beard & Lofgren, 1989; Spulber & Rutherford, 1983; Thy et al., 1990) without additional thermal input. The general crystallization temperature range indicated by the Ti-in-zircon thermometer (~700–800°C) (Ferry & Watson, 2007) suggests Snæfell zircon crystallized in conditions >100ºC cooler than the surrounding ambient bedrock, and therefore from magmas likely approximating solidus temperatures.

5.3 Trace element constraints on rhyolite source materials

In Iceland, the basaltic crust generally hydrates and metamorphoses to produce amphibolite. Therefore, identifying amphibole signatures (e.g., Sc and middle REEs are strongly partitioned into amphibole (Grimes et al., 2015)) is one way to evaluate depth and source of silicic melts. With the exception of three grains (out of ~100), all Snæfell zircon plots in the amphibole-poor region on the Ti vs. Sc/Yb diagram (Figure 4b) of Grimes et al. (2015), suggesting that their source melts are derived from a system that is not in equilibrium with amphibole. Amphibole-free source melts may be achieved through several mechanisms. The crust that hosts the Snæfell magmatic system is too cool to adequately circulate hydrothermal fluids to incite amphibolitization. These cool conditions may have persisted throughout the development of this older bedrock that was presumably once located in the active rift zone (e.g., the Northern volcanic zone (NVZ)). Mantle melts that undergo FC to produce rhyolites are

generally assumed to be too dry to stabilize amphibole (cf., Jónasson et al., 1992; Prestvik, 1980, 1982). Water-undersaturated melting experiments of metabasalt from 0.1 to 0.3 GPa yield silicic melts in equilibrium with an amphibole-free restite that are similar to metaluminous rhyolites characteristic of on-rift Icelandic rhyolites (Beard & Lofgren, 1989; Óskarsson et al., 1982; Spulber & Rutherford, 1983; Thy et al., 1990). While not a perfect match for Snaefell's mildly peraluminous melts, these experimental results support the idea that PM can generate non-amphibole-bearing, zircon-saturated rhyolites at middle-to-deep crust depths (0.1 to 0.3 GPa).

5.4 Oxygen isotopes in zircon and whole rock suggest a lack of crustal material incorporation

Zircon crystallizing from melt generated through closed-system fractionation of mantle-derived magma should have $\delta^{18}O=5.3\pm0.6‰$ (Valley et al., 1998, 2005). Zircons from Snæfell have $\delta^{18}O$ ranging from ~3.1 to 4.4‰. These values are lower than expected for mantle-equilibrated zircon, but within the typical range of $\delta^{18}O$ for Icelandic zircon; 90% of measured Icelandic zircon grains have $\delta^{18}O$ ranging from 0.2‰ to 4.7‰ (mean $\delta^{18}O$ of 3.0‰) (Carley et al., 2014).

Hattori and Muehlenbachs (1982) provide data for oxygen isotope ratios in the upper 3 km of the Icelandic crust. Low $\delta^{18}O$ basaltic bedrock is thought to arise (1) because the Icelandic mantle has uniquely low $\delta^{18}O$ (e.g., Thirlwall et al., 2006); or (2) through hydrothermal alteration by low-^{18}O water or contamination by materials affected by such water (e.g., Bindeman et al., 2008, 2012; Hattori and Muehlenbachs, 1982; Condomines et al., 1983). If the Icelandic mantle has low $\delta^{18}O$ (Scenario 1 above), then basalts erupted and intruded throughout Iceland's history—the rocks composing the bedrock—would retain that signature and the crust would have

low $\delta^{18}O$. The presence of olivine crystals with mantle-normal O isotope compositions in Icelandic basalts argues against an abnormally depleted Icelandic mantle. It is instead likely that low-^{18}O magmas in Iceland result from hydrothermal alteration by isotopically light meteoric water, or through anatexis or assimilation of such material (Scenario 2 above) (Gurenko et al., 2015; Bindeman et al., 2008, 2012).

Hydrothermal alteration by low-^{18}O meteoric water occurs in the upper few km of the crust in active rift zones—especially areas surrounding central volcanoes—where sufficient heat exists to drive circulation and facilitate isotopic diffusion to produce low-^{18}O bedrock. Iceland is constructed by persistent spreading-induced eruptions and occasional rift relocations. The Tertiary plateau lava sequence approaches ~10 km thick (Walker, 1964, 1974). Following the crust-building model of Pálmason (1986), Tertiary lavas erupted from now-extinct rifts, were buried by subsequent eruptions, subsided as they cooled and were rifted away from their spreading center, and experienced hydrothermal alteration within ~2 Myr of formation. Precipitation in Iceland appears to have been low-^{18}O throughout the last 16 Ma, although just how low has varied with climate over time (Carley et al., 2020). Therefore, it is conceivable that Icelandic bedrock at depth (>3 km) has low ^{18}O values due to hydrothermal alteration. Lavas produced in off-rift zones tend to have higher $\delta^{18}O$ values (e.g., Martin and Sigmarsson, 2007), and we expect the same to be true of the bedrock they build in the millions of years following their eruption, burial, and subsidence. However, contributions from these (or similar, now-defunct and buried) off-rift areas are far subordinate to the volume of crust added at and around the active rift zones.

Zircon $\delta^{18}O$ is lower than the $\delta^{18}O$ in melt from which it grows—for rhyolitic melt, the difference is roughly 1.8‰ at 850°C (Bindeman et al., 2012; Trail et al., 2009). Crystal-poor host

492 rhyolites of the Snæfell zircon grains have whole rock $\delta^{18}O$ of ~5.1 to 5.5‰, which overlap the
493 expected range of rhyolite $\delta^{18}O$ based on the above relationship. However, zircon textures, age
494 data, and compositions support the interpretation that Snæfell zircons are antecrysts (e.g., Bacon
495 & Lowenstern, 2005; Charlier et al., 2005; Miller et al., 2007; and many others)—crystals
496 derived from an earlier episode of magmatism and which are incorporated in a later pulse(s). If
497 we assume that the sampled rhyolites are broadly representative of the zircons' parental magmas,
498 O fractionation modelling can provide context for rhyolite petrogenesis.

499 Extended closed-system crystallization of mafic melt leads to an increase of roughly 0.5
500 to 1‰ in $\delta^{18}O$ in fractionated rhyolite melt (e.g., Bindeman, 2008; Trail et al., 2009; cf. Valley et
501 al., 2005). Pope et al. (2013) present a model for basalts at Krafla volcano in which a mantle-
502 derived basalt ($\delta^{18}O$=5.5‰) repeatedly assimilates ~15% melt from hydrothermally altered
503 bedrock ($\delta^{18}O$=-10‰) to produce a magma with final $\delta^{18}O$=4.7‰ over 15 Myr; however, it
504 should be noted that altered crust with $\delta^{18}O$ as low as -10‰ is unusual for Iceland as a whole
505 (Hattori & Muehlenbachs, 1982). Snæfell basalts have $\delta^{18}O$~5‰ (Hards et al., 2000). Results of
506 mass-balance modeling of ^{18}O fractionation between zircon and host melt based on the model of
507 Pope et al. (2013) are presented below (Figure 6) and in Supplemental Table S5. However,
508 interpretation based on such modeling is complicated by variability in the altered crust
509 (~2>$\delta^{18}O$>-10‰; Hattori & Muehlenbachs, 1982). As mentioned in section 5.3, evidence is
510 lacking for a hydrothermal system associated with Snæfell, and there is uncertainty regarding the
511 degree to which those conditions may have persisted throughout bedrock development—and in
512 mantle basalt (~4 to 5.5‰; e.g., Pope et al., 2013).

513 There are many pathways to the whole rock and zircon $\delta^{18}O$ compositions observed at
514 Snæfell. For example, zircon crystallizing from a melt composed of a 4:1 ratio of rhyolite melt

515 derived from fractional crystallization of mantle basalt ($\delta^{18}O$ ~5.5‰) and rhyolite melt derived
516 from anatexis of crust with $\delta^{18}O$~2‰ will have $\delta^{18}O$ ~3.5‰—as will zircon crystallizing from a
517 ~19:1 ratio of rhyolite melt derived from fractional crystallization of mantle basalt ($\delta^{18}O$~5.5‰)
518 and rhyolite melt derived from anatexis of crust with $\delta^{18}O$=-10‰ (Figure 6; Supplemental Table
519 S5).

520 These findings suggest that a dominant proportion of relatively high-$\delta^{18}O$ (i.e., near
521 mantle value) melt with minimal contribution from low-$\delta^{18}O$ recycled crust is required to
522 produce Snæfell silicic magmas that host zircon. This pathway to low-$\delta^{18}O$ melt is not unusual in
523 modern Iceland (e.g., Bindeman et al., 2012; Gurenko et al., 2015), except at off-rift Öræfajökull
524 at the southern end of the ÖVB (Carley et al., 2020) (Figure 1b), and may be achieved in one of
525 three ways: (1) Snæfell silicic melts result from closed-system fractional crystallization of
526 mantle-derived melts with $\delta^{18}O$~5‰; (2) crustal inputs are of a similar O isotopic composition as
527 any fresh mantle-derived melts such that any proportion of assimilated crust—even a dominant
528 one—does not leverage a significant shift in isotopic composition; or (3) a combination of both
529 occurred. Little intrasample variability in zircon $\delta^{18}O$ demonstrates behavior trending toward
530 closed-system. Open-system behavior could be accommodated only with approximately
531 homogeneous inputs from small batches of melt. Therefore, all these scenarios result in both
532 zircon and whole rock $\delta^{18}O$ compatible with our findings.

533 **Figure 6.** Potential pathways of rhyolite production at Snæfell that result in the observed zircon oxygen isotope
534 compositions. Left scenario utilizes a starting mantle $\delta^{18}O$ of 5.5‰; middle and right scenarios utilize mantle
535 $\delta^{18}O$=5.0‰ for comparison.
536

5.5 Hafnium isotopes in zircon—a case for deep-crust involvement?Hafnium isotope data further distinguish between fractional crystallization of new mantle melts vs. incorporation of pre-existing crust. Zircon ε_{Hf} from +13.3 to +16.3 in the Snæfell samples overlaps with—but extends to considerably higher values than—the range reported for basaltic magmas erupted from the Snæfell system (ε_{Hf} ~+13 to +13.5) and the propagating EVZ (ε_{Hf} ~+11 to +13.5) (Peate et al., 2010). Snæfell zircon ε_{Hf} is higher than in basalts from other modern off-rift zones, including Öræfajökull (ε_{Hf} ~+11 to +12) and overlaps the range (ε_{Hf} ~+13.5 to +19) of values from basalts erupted from modern established rifts (Peate et al., 2010; data re-reduced using the CHUR value of Bouvier et al., 2008 to be internally consistent with this study). Measured zircon Hf compositions in samples IESn1, IESn2, and IESn3 vary by ~2–2.5 epsilon units (Table 2; Figure 3c), which is typical for Icelandic systems (Padilla et al., 2016; Banik et al., 2018; Carley et al., 2020).

Icelandic magmas exhibit an apparent latitudinal difference between more- and less-radiogenic Hf isotope bedrock (and zircon), with less radiogenic compositions to the south (ε_{Hf} < ~+12 to +14) and more radiogenic compositions to the north (ε_{Hf} > ~+12 to +14) (Carley et al., 2020). The distribution of ε_{Hf} compositions appears to reflect a persistent distinction between the mantle that underlies northern and southern Iceland. The edifice of Snæfell unconformably overlies bedrock up to 10 Myr old (at depth) that erupted from the Northern volcanic zone (Figure 1) several million years after the Northern segment of the rift initiated (Martin et al., 2011). Thus, the crust that hosts Snæfell's magmatic system most likely resembles that generated from established rifts that erupt magmas with a MORB-dominant, more radiogenic Hf isotope composition. Regional heterogeneity of the underlying crust and mantle, along with slight deviations in spreading direction with respect to the rift axis, permits the Snæfell magmatic

560 system to be hosted in bedrock that has an isotopic composition with characteristics similar to
561 that of other NVZ-produced bedrock.

562 Icelandic volcanic systems typically display generally coherent radiogenic isotopic
563 compositions between basalt and rhyolite (e.g., Peate et al., 2010; Nicholson et al., 1991; Stecher
564 et al., 1999; Banik et al., 2018). A suite of mafic to rhyolitic samples at Snæfell reveals
565 indistinguishable Sr, Nd, and Pb isotope bulk rock compositions across the suite (Hards et al.,
566 2000)—however, bulk rock Hf isotope data currently exist only for basalts (ε_{Hf}~+12.9–13.3;
567 Peate et al., 2010). The correlation between ε_{Nd} and ε_{Hf} is generally strong globally (e.g.,
568 Vervoort & Blichert-Toft, 1999;$\varepsilon_{Hf(t)}=1.36 \times \varepsilon_{Nd(t)} + 3$), which was demonstrated for Icelandic
569 basalts by Peate et al. (2010). Further, Carley et al. (2020) demonstrated a correlation between
570 Icelandic whole rock and zircon Hf isotope values, and then developed mathematical
571 relationships to associate Icelandic whole rock Hf and Nd isotope values—$\varepsilon_{Hf}=(1.48 \times \varepsilon_{Nd}) +$
572 2.52; $r^2=0.65$—and zircon Hf isotope compositions. Isotopic values for whole rocks may then be
573 estimated in the absence of measured values using the above relationships.

574 Hards et al. (2000) and Peate et al. (2010) report whole rock Nd data for 6 and 7 Snæfell
575 samples, respectively. However, only one of these samples is a rhyolite; the remainder are
576 basalts. The data reported by Hards et al. (2000), including the rhyolite, do not include Hf
577 isotope compositions. We used published Nd isotope compositions and the calculations of Carley
578 et al. (2020), above, to determine approximate Hf isotope compositions for a sample of rhyolite
579 and additional basalt samples. We do not observe the expected correlation between Snæfell
580 whole rock rhyolite ε_{Nd} (measured) and zircon ε_{Hf} (measured) and between basalt ε_{Hf} (calculated)
581 and zircon ε_{Hf} (measured)(Figure 7). This discrepancy suggests that the zircon grains grew in

magmas with different Hf isotope compositions than those in which they were finally entrained and erupted. It also highlights the complicated isotopic nature of the Icelandic crust, mantle, and minerals therein.

Figure 7. Whole rock and zircon ε_{Hf} vs. whole rock ε_{Nd} for rhyolites from Snæfell and other Neovolcanic systems. Snæfell rhyolite and basalt from Hards et al. (2000) with calculated ε_{Hf} from measured ε_{Nd} following the method of Carley et al. (2020); Snæfell zircon from this study. Compositions from Snæfell basalts noted by the hatched field (Peate et al., 2010) and stars (Hards et al., 2000) for comparison. All other data from Carley et al. (2020). Array after Vervoort & Blichert-Toft (1999). Note that Hekla and Torfajökull are often considered more petrogenetically representative of the South Iceland Seismic Zone (SISZ) than the nearby Eastern rift zone.

Changes in mantle-crust interaction could potentially result in changes in Hf isotope compositions. Storck et al. (2020) demonstrate that mantle flux plays a key role in determining whether mantle melt or crustal contamination dominates in silicic petrogenesis. Early basaltic intrusions into the crust may cause only limited melting and assimilation but ensuing magma injections into progressively hotter crust might result in more extensive partial melting and assimilation of crustal material with time (Storck et al., 2020). If this model is applied to Snæfell, the slightly elevated zircon ε_{Hf} values in the young grains from IESn3 would result from crystallization in rhyolite derived from a higher fraction of anatectic melts from high-ε_{Hf} crust relative to older samples IESn1 and IESn2. However, the Snæfell zircon grains ultimately became entrained in magmas with comparably lower ε_{Hf} values. These host magmas would then need to be derived by a mechanism independent of magma flux—such as the involvement of substantial volumes of low-ε_{Hf} magma, likely from the mantle, on the scale of 10s to 100s of kyr—which is difficult to envision in this context. Another consideration is that the established

eruptive lifetime of Snæfell (~466–207 ka) may have started to wane by the time the IESn3 zircons crystallized ~266 ka. If Snæfell's plumbing system experienced a system-wide thermal energy decrease, as is hinted at by the low Ti concentrations (and thus cool crystallization Ts) in zircon, we would expect to see evidence of less anatexis in the form of lower ε_{Hf} values in the younger Snæfell zircons, not the higher ε_{Hf} values observed (Figures 3, 7). The shift of magmatism southward along the ÖVB toward Öræfajökull (Hards et al., 2000) supports the hypothesis of a diminished heat budget. A simpler and more plausible scenario for imparting higher-ε_{Hf} signatures to Snæfell zircon without also raising the bulk rock ε_{Hf} values is to crystallize and store zircons in melts generated by anatexis of deeper crust formed during an earlier stage of rifting.

The zircon Hf isotope compositions presented here argue against the presence and involvement of trapped continental crust under eastern Iceland (Foulger, 2006; Torsvik et al., 2015). If magmas from which Snæfell zircon grains crystallized were contaminated by the underlying continental lithosphere, then we would expect much lower ε_{Hf} values (e.g., Greenland zircon with $\varepsilon_{Hf(i)}<2.5$; Fisher & Vervoort, 2018), not the very high values observed here ($\varepsilon_{Hf}>\sim+13$; Figure 3). Based on these data, there is no continental crust under Snæfell, or—if present—it has not contributed enough during petrogenesis to imprint on the zircon isotopic record.

5.6 An updated petrogenetic model for Snæfell rhyolites

Hards et al. (2000) argue that neither partial melting (PM) of the tholeiitic bedrock nor pre-existing segregations of silicic material (observed as xenoliths in Snæfell basalts) can account for Snæfell's peralkaline rhyolites, and therefore propose that Snæfell rhyolites are

produced dominantly through fractional crystallization (FC). Hards et al. (2000) note that FC alone cannot account for all the compositional characteristics observed in Snæfell's rhyolites and posit that involvement of pre-existing crust is a subordinate—but detectable—presence in rhyolite petrogenesis. While we fundamentally agree with the interpretation of Hards et al. (2000), the zircon-based geochronologic, geochemical, and isotopic evidence presented here allow for an updated and more intricate view of rhyolite production at Snæfell. This detailed model of silicic petrogenesis at Snæfell must account for (1) the geochronology trends observed amongst zircon cores and mantles and between samples; (2) differences in magma conditions and evolution as inferred from zircon trace element concentrations and trends between the samples; (3) zircon and whole rock O isotope values lacking indications of a significant isotopically light component; and (4) zircon grains with Hf isotope compositions that are more radiogenic than those measured in Snæfell's basalts and modeled for Snæfell's rhyolites.

Zircon evidence suggests much longer magma residence times than have previously been observed in Neovolcanic Icelandic magma systems. Zircon CL images support zircon crystallization, residence, and remobilization with the presence of different zoning patterns between cores and mantles of grains and, in some cases, clear core/mantle boundaries (Figure 2). Zircon core ages average 10s to 100s of kyr older than mantles of grains extracted from the same samples. The overall range of crystallization ages is broadly synchronous with ages for other Snæfell eruptive units obtained via whole-rock geochronology. However, the ages obtained from both cores and mantles of zircon grains from samples IESn1 and IESn2 pre-date the oldest dated eruptive unit by at least 25 kyr (Figure 3a; Table 2).

Trace element concentrations of zircon grains derived from Snæfell rhyolites suggest crystallization from magmas with somewhat variable compositional histories. Zircon Hf and

650 REE concentrations (Figures 4 and 5) vary, likely as a result of crystallization in melts from a
651 range of evolutionary paths. It appears that none of these melts were influenced by the presence
652 of amphibole based on the somewhat variable but generally low concentrations of Sc (Figure 4).
653 Finally, Ti concentrations suggest zircon crystallization in cooler conditions than are typical in
654 Iceland (Figure 4), likely as a result of late-stage saturation in melts that lost heat to a somewhat
655 cool crust given the distance from both the active rift and the hotspot (Martin & Sigmarsson,
656 2010). Titanium concentrations increase toward the surfaces of grains from samples IESn2 (3
657 ppm increase; ~50°C) and IESn3 (4 ppm increase; ~70°C), indicating a late-stage heating event
658 likely associated with introduction of hotter mafic material. Reheating likely led to rejuvenation
659 and mixing of silicic magmas in a range of states (e.g., sub-solidus, crystal mush, mostly melt)
660 repeatedly throughout the system's lifetime. These thermal perturbations may have destabilized
661 magmas and triggered eruptions.

662 Thermal involvement of hotter mafic material and the operation of open-system
663 processes opens a critical door to understanding the overall genesis of rhyolites at Snæfell.
664 Oxygen isotope values of zircons ($\delta^{18}O$~3–4‰) and their host rocks ($\delta^{18}O$~5–5.5‰) indicate a
665 lack of substantial involvement of low-^{18}O material commonly associated with hydrothermally
666 altered bedrock in Iceland. As discussed in Section 5.3 this could mean:

667 (1) these materials were formed from FC of fresh mantle melts with $\delta^{18}O$~5–5.5‰;

668 (2) these materials result from assimilation and/or anatexis of Icelandic bedrock that
669 escaped substantial hydrothermal interaction with low-^{18}O water and therefore has not
670 been imprinted with a low-^{18}O signature;

671 (3) some combination of these two end-member processes that results in an assimilation-
672 fraction crystallization (AFC) hybrid magma; or

673 (4) the zircons detailed in this study may be xenocrystic and therefore do not provide
674 constraint on the petrogenesis of Snæfell rhyolites, but rather elucidate intra-crustal
675 differentiation processes.

676 Scenario 1 is a tidy explanation and fits the standard explanation for rhyolite formation in
677 off-rift areas (e.g., Jónasson, 2007; Martin & Sigmarsson, 2010; Schattel et al., 2014). Scenario 2
678 is attractive because of the high probability that repeated injections of basalt could lead to
679 localized, small-batch melting of the bedrock. Scenario 3 is also highly plausible and has been
680 demonstrated at other volcanic systems, both active and extinct (e.g. Macdonald et al., 1987;
681 Nicholson et al., 1991; Banik et al., 2018). Scenario 4 is improbable—while some zircon ages
682 predate edifice-building eruptions at Snæfell, they are generally synchronous with the Snæfell
683 and occur within a geologically reasonable timeframe for zircon crystallization predating
684 eruption (e.g., >100 kyr, Reid et al., 1997; ~300 kyr, Claiborne et al., 2010). It is more difficult
685 to explain off-rift, rhyolite-generating, zircon saturated magmas in the same location as Snæfell
686 that persisted for 100s of kyr. We therefore focus on Scenarios 1–3 moving forward.

687 In evaluating each of Scenarios 1–3, we must bear in mind the isotopic complexities in
688 the zircon and whole-rock records. Hafnium isotope compositions in Snæfell zircon grains
689 suggest crystallization from melts with a more radiogenic component than is observed in Snæfell
690 basalts (which also have $\delta^{18}O$~5‰). In order to achieve the observed O isotope values in Snæfell
691 rhyolites, the radiogenic Hf measured in the zircon grains must originate from a source that also
692 has approximately mantle values for $\delta^{18}O$ (~5‰) and ε_{Hf}~14–19—a composition similar to that

693 of NVZ basalts (e.g. Peate et al., 2010 and references therein). Scenario 1 presented above seems
694 to satisfy all the zircon geochemical observations presented here yet cannot account for the
695 difference in Hf isotope compositions between the Snæfell zircons and Snæfell whole rock (both
696 measured and modeled; Figure 7). The involvement of hotter, more mafic material at the end of
697 the Snæfell zircons' crystallization lends support to Scenario 2. However, the degree to which
698 the bedrock surrounding the magmatic system >10 km under Snæfell escaped significant impact
699 by hydrothermal alteration in the first few million years of its existence—when it was hotter and
700 closer to the surface to allow groundwater circulation—is difficult to assess. In theory, the
701 metabasaltic crust may have passed the amphibole breakdown curve and generated fluid-absent
702 anatectic rhyolite melts to generate the older zircon cores. Subsequent thermal episodes may
703 have occurred ~350 kyr and ~265 kyr ago resulting in zircon crystallization from defrosted
704 silicic segregations/intrusions, followed by and eruption. Alternate scenarios may be able to
705 satisfy the requirements listed above. However, Scenario 3—the AFC model—draws on the
706 strengths of the two end-member processes and is thus the most geologically reasonable way to
707 produce the observed zircon geochemical characteristics within the constraints of whole-rock
708 geochemical parameters.

709 Rhyolite petrogenesis at Snæfell likely occurs in a modified AFC scenario whereby
710 extended fractional crystallization of new, mantle-derived magmas dominates over assimilation
711 of volumetrically minor and slightly varying amounts of low-^{18}O, high-ε_{Hf} bedrock (Figure 8;
712 Supplemental Table S7). This supports the conclusion of Hards et al. (2000) while providing new
713 details about the amounts and compositions of the anatectic melts and a more detailed history of
714 the magmatic system. Snæfell zircon CL textures, evidence of late-stage pre-eruptive heating,

715 and ages support a system in which crystallization, potential dormancy in sub-solidus conditions,
716 and periodic rejuvenation, ultimately culminating in eruption, persisted for 100s of kyr.

717

718 **Figure 8.** Model for Snæfell rhyolite petrogenesis based on zircon data. Amounts and values of ε_{Hf} and $\delta^{18}O$ are
719 general; see text for discussion of uncertainty regarding crustal isotopic composition. (a) Snæfell magmatism begins
720 before the first edifice-building eruption at 466 ka. (a1) Rhyolite results dominantly from FC of fresh mantle melts
721 with subordinate contributions from assimilation of low-$\delta^{18}O$, high-ε_{Hf} crust. (b) Rhyolite-hosted zircon experiences
722 subsolidus conditions. (c) Rejuvenation allows additional zircon saturation and growth, as well as potential for
723 mixing of rhyolite magma batches and introduction of anatectic melt. Cycles of zircon growth, subsolidus
724 quiescence, and rejuvenation may continue for some time prior to eruption. (d) Rhyolite destabilization and
725 eruption. Zircon grains record multiple pulses of growth over 10s to 100s of kyr and are hosted in rhyolites with
726 lower ε_{Hf}—but similar $\delta^{18}O$—characteristics.

727 ## 6 Conclusions

728 The first ever zircon-based constraints on the timing, longevity, and petrogenetic processes
729 associated with production of rhyolites at Snæfell volcano, Iceland, include the following:

730 - Zircon ages range from ~545 ka to ~265 ka, with ages between grain cores and mantles
731 differing by ~100 to 200 kyr within a single sample. This suggests that zircon
732 crystallization, sub-solidus storage, and remobilization on timescales up to ~200 kyr was
733 common at Snæfell. These absolute ages are consistent with zircon CL internal zoning
734 and textures;

735 - Zircon trace element concentrations suggest crystallization occurred in relatively cool
736 magmas derived from amphibole-free sources with minimal fractionation following

737 zircon saturation. Introduction of hotter magma initiated remobilization, and ultimately
738 eruption, of silicic magmas;

739 • Zircon $\delta^{18}O$ ranges from ~3.5–~4‰—consistent with crystallization from a silicic
740 magma dominantly derived from fractional crystallization of primitive mantle melt with
741 variable but minor input from an ^{18}O-depleted source; and

742 • Zircon ε_{Hf} ranges from ~+13 to ~+17 (sample averages: ~+14.1 to +14.7), which is
743 substantially more radiogenic than measured Snæfell basalt (ε_{Hf}~+12.9–13.3; Peate et al.,
744 2010) or modeled rhyolite (ε_{Hf}=+13.3).

745 We invoke a petrogenetic model whereby repeated injections of primitive mantle-derived
746 basalts undergo fractional crystallization, with a minor component of assimilated bedrock, to
747 produce small volumes of rhyolite melt. These rhyolites are periodically rejuvenated through
748 additional mantle magma additions, then erupt when disturbed by substantially hotter injections.
749 These zircon data allow for a novel view of rhyolite petrogenesis at Snæfell and provide more
750 detailed insight on processes operating over magmatic timescales far longer than those
751 previously reported for the Snæfell magmatic system and other Neovolcanic magmatic system in
752 Iceland.

753

754 **Acknowledgments, Samples, and Data**

755 The authors are not aware of any real or perceived financial conflicts of interest or affiliation
756 conflicts of interest pertaining to this research. Data used for Iceland zircon comparisons are
757 available in Carley et al. (2014), Banik et al. (2018), and Carley et al. (2020). Original data from

this research is archived at EarthChem [https://doi.org/10.26022/IEDA/111737]. Funding for this research from Illinois State University (TJB) and Lafayette College (TLC). WiscSIMS is partly supported by NSF (EAR03-19230, EAR10-53466, EAR13-55590). Thoughtful and constructive reviews from J. Storck and two anonymous reviewers greatly improved this manuscript. Thank you to M. Edmonds and C. Micucci for editorial assistance. We are grateful to J. Valley and N. Kita for facilitating analytical time and K. Kitajima for analytical assistance at WiscSIMS. R. Lam provided invaluable analytical support at Memorial University, Newfoundland. Thank you, all.

References

Bachmann, O., Charlier, B. L. A., & Lowenstern, J. B. (2007). Zircon crystallization and recycling in the magma chamber of the rhyolitic Kos Plateau Tuff (Aegean arc). *Geology*, *35*(1), 73–76. https://doi.org/10.1130/G23151A.1

Bachmann, O., & Bergantz, G. W. (2009). Rhyolites and their Source Mushes across Tectonic Settings. *Journal of Petrology*, *49*(12), 2277–2285. https://doi.org/10.1093/petrology/egn068

Bachmann, O., Dungan, M. A., & Lipman, P. W. (2002). The Fish Canyon magma body, San Juan volcanic field, Colorado: rejuvenation and eruption of an upper-crustal batholith. *Journal of Petrology*, *43*(8), 1469–1503. https://doi.org/10.1093/petrology/43.8.1469

Bacon, C. R., & Lowenstern, J. B. (2005). Late Pleistocene granodiorite source for recycled zircon and phenocrysts in rhyodacite lava at Crater Lake, Oregon. *Earth and Planetary Science Letters*, *233*(3), 277–293. https://doi.org/10.1016/j.epsl.2005.02.012

Baertschi, P. (1976). Absolute ^{18}O content of standard mean ocean water. *Earth and Planetary*

Science Letters, *31*(3), 341–344. https://doi.org/10.1016/0012-821X(76)90115-1.

Banik, T. J., Miller, C. F., Fisher, C. M., Coble, M. A., & Vervoort, J. D. (2018). Magmatic-tectonic control on the generation of silicic magmas in Iceland: Constraints from Hafnarfjall-Skarðsheiði volcano. *Lithos*, *318–319*, 326–339. https://doi.org/10.1016/j.lithos.2018.08.022

Beard, J. S., & Lofgren, G. E. (1989). Effect of Water on the Composition of Partial Melts of Greenstone and Amphibolite. *Science*, *244*(4901), 195–197. https://doi.org/10.1126/science.244.4901.195

Bindeman, I. (2008). Oxygen Isotopes in Mantle and Crustal Magmas as Revealed by Single Crystal Analysis. *Reviews in Mineralogy and Geochemistry*, *69*(1), 445–478. https://doi.org/10.2138/rmg.2008.69.12

Bindeman, I., Gurenko, A., Sigmarsson, O., & Chaussidon, M. (2008). Oxygen isotope heterogeneity and disequilibria of olivine crystals in large volume Holocene basalts from Iceland: Evidence for magmatic digestion and erosion of Pleistocene hyaloclastites. *Geochimica et Cosmochimica Acta*, *72*(17), 4397–4420. https://doi.org/10.1016/J.GCA.2008.06.010

Bindeman, I., Gurenko, A., Carley, T., Miller, C., Martin, E., & Sigmarsson, O. (2012). Silicic magma petrogenesis in Iceland by remelting of hydrothermally altered crust based on oxygen isotope diversity and disequilibria between zircon and magma with implications for MORB. *Terra Nova*, *24*(3), 227–232. https://doi.org/10.1111/j.1365-3121.2012.01058.x

Black, L. P., Kamo, S. L., Allen, C. M., Davis, D. W., Aleinikoff, J. N., Valley, J. W., et al. (2004). Improved $^{206}Pb/^{238}U$ microprobe geochronology by the monitoring of a trace-element-related matrix effect; SHRIMP, ID–TIMS, ELA–ICP–MS and oxygen isotope

804 documentation for a series of zircon standards. *Chemical Geology*, *205*(1–2), 115–140.
805 https://doi.org/10.1016/j.chemgeo.2004.01.003
806 Bouvier, A., Vervoort, J. D., & Patchett, P. J. (2008). The Lu–Hf and Sm–Nd isotopic
807 composition of CHUR: Constraints from unequilibrated chondrites and implications for the
808 bulk composition of terrestrial planets. *Earth and Planetary Science Letters*, *273*(1–2), 48–
809 57. https://doi.org/10.1016/j.epsl.2008.06.010
810 Carley, T.L., Miller, C. F., Sigmarsson, O., Coble, M. A., Fisher, C. M., Hanchar, J. M., et al.
811 (2017). Detrital zircon resolve longevity and evolution of silicic magmatism in extinct
812 volcanic centers: A case study from the East Fjords of Iceland. *Geosphere*, *13*(5), 1640–
813 1663. https://doi.org/10.1130/GES01467.1
814 Carley, T. L., Miller, C. F., Wooden, J. L., Bindeman, I. N., & Barth, A. P. (2011). Zircon from
815 historic eruptions in Iceland: reconstructing storage and evolution of silicic magmas.
816 *Mineralogy and Petrology*, *102*(1–4), 135–161. https://doi.org/10.1007/s00710-011-0169-3
817 Carley, T. L., Miller, C. F., Wooden, J. L., Padilla, A. J., Schmitt, A. K., Economos, R. C., et al.
818 (2014). Iceland is not a magmatic analog for the Hadean: Evidence from the zircon record.
819 *Earth and Planetary Science Letters*, *405*, 85–97. https://doi.org/10.1016/j.epsl.2014.08.015
820 Carley, T. L., Miller, C. F., Fisher, C. M., Hanchar, J. M., Vervoort, J. D., Schmitt, A. K., et al.
821 (2020). Petrogenesis of silicic magmas in Iceland through space and time: The isotopic
822 record preserved in zircon and whole rocks. *Journal of Geology*, *128*, 1–28.
823 https://doi.org/10.1086/706261
824 Carmichael, I. S. E. (1964). The petrology of Thingmuli, a Tertiary volcano in eastern Iceland.
825 *Journal of Petrology*, *5*(3), 435–460. https://doi.org/10.1093/petrology/5.3.435
826 Charlier, B. L. A., Wilson C. J. N., Lowenstern, J. B., Blake, S., Van Calsteren, P. W., &

827 Davidson, J. P. (2005). Magma Generation at a Large, Hyperactive Silicic Volcano (Taupo,
828 New Zealand) Revealed by U-Th and U-Pb Systematics in Zircons. *Journal of Petrology*,
829 *46*(1), 3–32. https://doi.org/10.1093/petrology/egh060
830 Chekol, T. A., Kobayashi, K., Yokoyama, T., Sakaguchi, C., & Nakamura, E. (2011).
831 Timescales of magma differentiation from basalt to andesite beneath Hekla Volcano,
832 Iceland: Constraints from U-series disequilibria in lavas from the last quarter-millennium
833 flows. *Geochimica et Cosmochimica Acta*, *75*(1), 256–283.
834 https://doi.org/10.1016/j.gca.2010.10.001
835 Cherniak, D. J., & Watson, E. B. (2003). Diffusion in Zircon. *Reviews in Mineralogy and*
836 *Geochemistry*, *53*(1), 113–143. https://doi.org/10.2113/0530113
837 Claiborne, L. L., Miller, C. F., Flanagan, D. M., Clynne, M. A., & Wooden, J. L. (2010). Zircon
838 reveals protracted magma storage and recycling beneath Mount St. Helens. *Geology*,
839 *38*(11), 1011–1014. https://doi.org/10.1130/G31285.1
840 Coble, M. A., Vazquez, J. A., Barth, A. P., Wooden, J., Burns, D., Kylander-Clark, A., et al.
841 (2018). Trace Element Characterisation of MAD-559 Zircon Reference Material for Ion
842 Microprobe Analysis. *Geostandards and Geoanalytical Research*, (42), 481–497.
843 https://doi.org/10.1111/ggr.12238
844 Condomines, M., Grövold, K., Hooker, P. J., Muehlenbachs, K., O'Nions, R. K., Óskarsson, N.,
845 & Oxburgh, E. R. (1983). Helium, oxygen, strontium and neodymium isotopic relationships
846 in Icelandic volcanics. *Earth and Planetary Science Letters*, *66*, 125–136.
847 https://doi.org/10.1016/0012-821X(83)90131-0
848 Cooper, K. M, Sims, K. W. W., Eiler, J. M., & Banerjee, N. (2016) Timescales of storage and
849 recycling of crystal mush at Krafla Volcano, Iceland. *Contributions to Mineralogy and*

Petrology, 171(6), 54. https://doi.org/10.1007/s00410-016-1267-3

Darbyshire, F. A., White, R. S., & Priestley, K. F. (2000). Structure of the crust and uppermost mantle of Iceland from a combined seismic and gravity study. *Earth and Planetary Science Letters*, *181*(3), 409–428. https://doi.org/10.1016/S0012-821X(00)00206-5

DeMets, C., Gordon, R. G., & Argus, D. F. (2010). Geologically current plate motions. *Geophysical Journal International*, *181*(1), 1–80. https://doi.org/10.1111/j.1365-246X.2009.04491.x

Ferry, J. M., & Watson, E. B. (2007). New thermodynamic models and revised calibrations for the Ti-in-zircon and Zr-in-rutile thermometers. *Contributions to Mineralogy and Petrology*, *154*(4), 429–437. https://doi.org/10.1007/s00410-007-0201-0

Finch, R. J., & Hanchar, J. (2003). Structure and Chemistry of Zircon and Zircon-Group Minerals. *Reviews in Mineralogy and Geochemistry*, *53*(1), 1–25. https://doi.org/10.2113/0530001

Fisher, C. M., & Vervoort, J. D. (2018). Using the magmatic record to constrain the growth of continental crust—The Eoarchean zircon Hf record of Greenland. *Earth and Planetary Science Letters*, *488*, 79–91. https://doi.org/10.1016/j.epsl.2018.01.031

Fisher, C. M., Hanchar, J. M., Samson, S. D., Dhuime, B., Blichert-Toft, J., Vervoort, J. D., & Lam, R. (2011). Synthetic zircon doped with hafnium and rare earth elements: A reference material for in situ hafnium isotope analysis. *Chemical Geology*, *286*(1–2), 32–47. https://doi.org/10.1016/J.CHEMGEO.2011.04.013

Fisher, C. M., Vervoort, J. D., & DuFrane, S. A. (2014). Accurate Hf isotope determinations of complex zircons using the “laser ablation split stream” method. *Geochemistry, Geophysics, Geosystems*, *15*(1). https://doi.org/10.1002/2013GC004962

873 Folkes, C. B., de Silva, S. L., Schmitt, A. K., & Cas, R. A. F. (2011). A reconnaissance of U-Pb
874 zircon ages in the Cerro Galán system, NW Argentina: Prolonged magma residence, crystal
875 recycling, and crustal assimilation. *Journal of Volcanology and Geothermal Research*,
876 *206*(3), 136–147. https://doi.org/10.1016/j.jvolgeores.2011.06.001
877 Foulger, G. R. (2006). Older crust underlies Iceland. *Geophysical Journal International*, *165*(2),
878 672–676. https://doi.org/10.1111/j.1365-246X.2006.02941.x
879 Furman, T., Frey, F. A., & Meyer, P. S. (1992). Petrogenesis of Evolved Basalts and Rhyolites at
880 Austurhorn, Southeastern Iceland: the Role of Fractional Crystallization. *Journal of*
881 *Petrology*, *33*(6), 1405–1445. https://doi.org/10.1093/petrology/33.6.1405
882 Gardner, J. E., Layer, P. W., & Rutherford, M. J. (2002). Phenocrysts versus xenocrysts in the
883 youngest Toba Tuff: Implications for the petrogenesis of 2800 km3 of magma. *Geology*,
884 *30*(4), 347–350. https://doi.org/10.1130/0091-7613(2002)030<0347:PVXITY>2.0.CO;2
885 Grimes, C. B., Wooden, J. L., Cheadle, M. J., & John, B. E. (2015). "Fingerprinting" tectono-
886 magmatic provenance using trace elements in igneous zircon. *Contributions to Mineralogy*
887 *and Petrology*, *170*(5–6), 1–26. https://doi.org/10.1007/s00410-015-1199-3
888 Gudmundsson, M. T., & Högnadóttir, T. (2007). Volcanic systems and calderas in the
889 Vatnajökull region, central Iceland: Constraints on crustal structure from gravity data.
890 *Journal of Geodynamics*, *43*(1), 153–169.
891 https://doi.org/https://doi.org/10.1016/j.jog.2006.09.015
892 Guillou, H., Van Vliet-Lanoë, B., Guðmundsson, A., & Nomade, S. (2010). New unspiked K–Ar
893 ages of Quaternary sub-glacial and sub-aerial volcanic activity in Iceland. *Quaternary*
894 *Geochronology*, *5*(1), 10–19. https://doi.org/10.1016/J.QUAGEO.2009.08.007
895 Guillou, H., Scao, V., Nomade, S., Van Vliet-Lanoë, B., Liorzou, C., & Guðmundsson, Á.

(2019). 40Ar/39Ar dating of the Thorsmork ignimbrite and Icelandic sub-glacial rhyolites. *Quaternary Science Reviews*, *209*, 52–62. https://doi.org/https://doi.org/10.1016/j.quascirev.2019.02.014

Gunnarsson, B., Marsh, B. D., & Taylor, H. P. (1998). Generation of Icelandic rhyolites: silicic lavas from the Torfajökull central volcano. *Journal of Volcanology and Geothermal Research*, *83*(1–2), 1–45. https://doi.org/10.1016/S0377-0273(98)00017-1

Gurenko, A. A., Bindeman, I. N., & Sigurdsson, I. A. (2015). To the origin of Icelandic rhyolites: insights from partially melted leucocratic xenoliths. *Contributions to Mineralogy and Petrology*, *169*(5), 49. https://doi.org/10.1007/s00410-015-1145-4

Halliday, A. N., Mahood, G. A., Holden, P., Metz, J. M., Dempster, T. J., & Davidson, J. P. (1989). Evidence for long residence times of rhyolitic magma in the Long Valley magmatic system: the isotopic record in precaldera lavas of Glass Mountain. *Earth and Planetary Science Letters*, *94*(3), 274–290. https://doi.org/10.1016/0012-821X(89)90146-5

Hanan, B. B., & Schilling, J.-G. (1997). The dynamic evolution of the Iceland mantle plume: the lead isotope perspective. *Earth and Planetary Science Letters*, *151*(1–2), 43–60. https://doi.org/10.1016/S0012-821X(97)00105-2

Hardarson, B. S., & Fitton, J. G. (1997). Mechanisms of crustal accretion in Iceland. *Geology*, *25*(11), 1043–1046. https://doi.org/10.1130/0091-7613(1997)025<1043:MOCAII>2.3.CO;2

Hards, V.L, Kempton, P. D., Thompson, R. N., & Greenwood, P. B. (2000). The magmatic evolution of the Snæfell volcanic centre; an example of volcanism during incipient rifting in Iceland. *Journal of Volcanology and Geothermal Research*, *99*(1), 97–121. https://doi.org/10.1016/S0377-0273(00)00160-8

Hards, V. L. (1995). *The evolution of the Snaefell Volcanic Centre, eastern Iceland.* Durham

919 University. Retrieved from http://etheses.dur.ac.uk/1452/
920 Hattori, K., & Muehlenbachs, K. (1982). Oxygen Isotope Ratios of the Icelandic Crust. *Journal*
921 *of Geophysical Research*, *87*(B8), 6559–6565. https://doi.org/10.1029/JB087iB08p06559
922 Helgason, J., Duncan, R. A., & Guðmundsson, A. (2005). Kárahnjúkar Hydroelectric Project,
923 Ar–Ar age dating of the Snæfell volcanic center. *Report for prepared by Ekra Geological*
924 *Consulting for the National Power Company of Iceland*.
925 Hildreth, W. (2004). Volcanological perspectives on Long Valley, Mammoth Mountain, and
926 Mono Craters: several contiguous but discrete systems. *Journal of Volcanology and*
927 *Geothermal Research*, *136*(3), 169–198. https://doi.org/10.1016/j.jvolgeores.2004.05.019
928 Hjartarson, Á., & Sæmundsson, K. (2014). Geological Map of Iceland. Bedrock. 1:600 000.
929 Iceland GeoSurvey (ÍSOR).
930 Höskuldsson, Á., & Imsland, P. (1998). Snæfell–Eldfjall á gosbelti framtíðar (Geology of
931 Snæfell, an intraplate volcano in Eastern Iceland). *Glettingur*, *8*, 22–30.
932 Höskuldsson, Á., Óskarsson, N., & Imsland, P. (1996). Snæfell, ágrip af jarðfræði og kvikuþróun
933 (in Icelandic). *Geoscience Society of Iceland Spring Meeting*.
934 Ivarsson, G. (1992). *Geology and petrochemistry of the Torfajokull central volcano in Central*
935 *South Iceland, in association with the Icelandic Hot Spot and Rift Zones*. University of
936 Hawaii.
937 Jakobsson, S. P., Jónasson, Kristján, & Sigurdsson, I. A. (2008). The three igneous rock series of
938 Iceland. *Jökull*, *58*, 117–138.
939 Jóhannesson, H., & Sæmundsson, K. (2009). Geological Map of Iceland. 1:600,000. Bedrock
940 geology. Reykjavík, Iceland: Icelandic Institute of Natural History.
941 Jónasson, K. (1994). Rhyolite volcanism in the Krafla central volcano, north-east Iceland.

Bulletin of Volcanology, *56*, 516–528. https://doi.org/10.1007/BF00302832

Jónasson, K. (2007). Silicic volcanism in Iceland: Composition and distribution within the active volcanic zones. *Journal of Geodynamics*, *43*(1), 101–117. https://doi.org/10.1016/j.jog.2006.09.004

Jónasson, K., Holm, P., & Pederson, K. (1992). Petrogenesis of Silicic Rocks from the Króksfjörður Central Volcano, NW Iceland. *Journal of Geophysical Research*, *33*, 1345–1369. https://doi.org/10.1093/petrology/33.6.1345

Kita, N. T., Ushikubo, T., Fu, B., & Valley, J. W. (2009). High precision SIMS oxygen isotope analysis and the effect of sample topography. *Chemical Geology*, *264*(1–4), 43–57. https://doi.org/10.1016/j.chemgeo.2009.02.012

Kitagawa, H., Kobayashi, K., Makishima, A., & Nakamura, E. (2008). Multiple Pulses of the Mantle Plume: Evidence from Tertiary Icelandic Lavas. *Journal of Petrology*, *49*(7), 1365–1396. https://doi.org/10.1093/petrology/egn029

Klemetti, E. W., & Clynne, M. A. (2014). Localized Rejuvenation of a Crystal Mush Recorded in Zircon Temporal and Compositional Variation at the Lassen Volcanic Center, Northern California. *PLOS ONE*, *9*(12), e113157. https://doi.org/10.1371/journal.pone.0113157

Kokfelt, T. F., Hoernle, K., Hauff, F., Fiebig, J., Werner, R., & Garbe-Schönberg, D. (2006). Combined Trace Element and Pb-Nd-Sr-O Isotope Evidence for Recycled Oceanic Crust (Upper and Lower) in the Iceland Mantle Plume. *Journal of Petrology*, *47*(9), 1705–1749. https://doi.org/10.1093/petrology/egl025

Kokfelt, T. F., Hoernle, K., Lundstrom, C., Hauff, F., & van den Bogaard, C. (2009). Time-scales for magmatic differentiation at the Snaefellsjökull central volcano, western Iceland: constraints from U–Th–Pa–Ra disequilibria in post-glacial lavas. *Geochimica et*

Cosmochimica Acta 73(4), 1120–1144. https://doi.org/10.1016/j.gca.2008.11.021

Lowenstern, J. B., Persing, H. M., Wooden, J. L., Lanphere, M., Donnelly-Nolan, J., & Grove, T. L. (2000). U–Th dating of single zircons from young granitoid xenoliths: new tools for understanding volcanic processes. *Earth and Planetary Science Letters*, *183*(1), 291–302. https://doi.org/10.1016/S0012-821X(00)00273-9

Ludwig, K. R. (2009). SQUID 2, A User's Manual. *Berkeley Geochronology Center Special Publication*, 100.

Ludwig, K. R. (2012). Isoplot 3.75, A Geochronological Toolkit for Excel. *Berkeley Geochronology Center Special Publication*, 75.

Macdonald, R., Sparks, R. S. J., Sigurdsson, H., Mattey, D. P., McGarvie, D. W., & Smith, R. L. (1987). The 1875 eruption of Askja volcano, Iceland: combined fractional crystallization and selective contamination in the generation of rhyolitic magma. *Mineralogical Magazine*, *51*(360), 183–202. https://doi.org/10.1180/minmag.1987.051.360.01

Maclennan, J. (2019). Mafic tiers and transient mushes: evidence from Iceland. *Philosophical Transactions of the Royal Society A: Mathematical, Physical and Engineering Sciences*, *377*(2139), 20180021. https://doi.org/10.1098/rsta.2018.0021

Mahon, K. I. (1996). The New "York" Regression: Application of an Improved Statistical Method to Geochemistry. *International Geology Review*, *38*(4), 293–303. https://doi.org/10.1080/00206819709465336

Mahood, G. A. (1990). Second reply to comment of R.S.J. Sparks, H.E. Huppert and C.J.N. Wilson on "Evidence for long residence times of rhyolitic magma in the Long Valley magmatic system: the isotopic record in the precaldera lavas of Glass Mountain." *Earth and Planetary Science Letters*, *99*(4), 395–399. https://doi.org/10.1016/0012-821X(90)90145-N

988 Manning, C. J., & Thirlwall, M. F. (2014). Isotopic evidence for interaction between Öræfajökull
989 mantle and the Eastern Rift Zone, Iceland. *Contributions to Mineralogy and Petrology*,
990 *167*(1), 959. https://doi.org/10.1007/s00410-013-0959-1
991 Marsh, B. D., Gunnarsson, B., Congdon, R., & Carmody, R. (1991). Hawaiian basalt and
992 Icelandic rhyolite: Indicators of differentiation and partial melting. *Geologische Rundschau*,
993 *80*(2), 481–510. https://doi.org/10.1007/BF01829378
994 Martin, E., & Sigmarsson, O. (2007). Crustal thermal state and origin of silicic magma in
995 Iceland: the case of Torfajökull, Ljósufjöll and Snæfellsjökull volcanoes. *Contributions to*
996 *Mineralogy and Petrology*, *153*, 593–605. https://doi.org/10.1007/s00410-006-0165-5
997 Martin, E., & Sigmarsson, O. (2010). Thirteen million years of silicic magma production in
998 Iceland: Links between petrogenesis and tectonic settings. *Lithos*, *116*(1–2), 129–144.
999 https://doi.org/10.1016/j.lithos.2010.01.005
1000 Martin, E., Paquette, J. L., Bosse, V., Ruffet, G., Tiepolo, M., & Sigmarsson, O. (2011).
1001 Geodynamics of rift–plume interaction in Iceland as constrained by new $^{40}Ar/^{39}Ar$ and in
1002 situ U–Pb zircon ages. *Earth and Planetary Science Letters*, *311*(1–2), 28–38.
1003 https://doi.org/10.1016/j.epsl.2011.08.036
1004 Mattsson, H. B., & Oskarsson, N. (2005). Petrogenesis of alkaline basalts at the tip of a
1005 propagating rift: Evidence from the Heimaey volcanic centre, south Iceland. *Journal of*
1006 *Volcanology and Geothermal Research*, *147*(3), 245–267.
1007 https://doi.org/10.1016/j.jvolgeores.2005.04.004
1008 McDonough, W. F., & Sun, S. -s. (1995). The composition of the Earth. *Chemical Geology*,
1009 *120*(3–4), 223–253. https://doi.org/10.1016/0009-2541(94)00140-4
1010 McGarvie, D. (2009). Rhyolitic volcano–ice interactions in Iceland. *Journal of Volcanology and*

1011 *Geothermal Research*, *185*(4), 367–389. https://doi.org/10.1016/j.jvolgeores.2008.11.019
1012 Miller, J. S., & Wooden, J. L. (2004). Residence, Resorption and Recycling of Zircons in Devils
1013 Kitchen Rhyolite, Coso Volcanic Field, California. *Journal of Petrology*, *45*(11), 2155–
1014 2170. https://doi.org/10.1093/petrology/egh051
1015 Miller, J. S., Matzel, J. E. P., Miller, C. F., Burgess, S. D., & Miller, R. B. (2007). Zircon growth
1016 and recycling during the assembly of large, composite arc plutons. *Journal of Volcanology*
1017 *and Geothermal Research*, *167*(1), 282–299.
1018 https://doi.org/10.1016/j.jvolgeores.2007.04.019
1019 Mussett, A. E., Ross, J. G., & Gibson, I. L. (1980). 40Ar/39Ar dates of eastern Iceland lavas.
1020 *Geophysical Journal International*, *60*(1), 37–52. https://doi.org/10.1111/j.1365-
1021 246X.1980.tb02579.x
1022 Nicholson, H., Condomines, M., Fitton, J. G., Fallick, A. E., Grönvold, K., & Rogers, G. (1991).
1023 Geochemical and Isotopic Evidence for Crustal Assimilation Beneath Krafla, Iceland.
1024 *Journal of Petrology*, *32*(5), 1005–1020. https://doi.org/10.1093/petrology/32.5.1005
1025 Óskarsson, N., Sigvaldason, G. E., & Steinthorsson, S. (1982). A dynamic model of rift zone
1026 petrogenesis and the regional petrology of Iceland. *Journal of Petrology*, *23*(1), 28–74.
1027 https://doi.org/10.1093/petrology/23.1.28
1028 Padilla, A. J., Miller, C. F., Carley, T. L., Economos, R. C., Schmitt, A. K., Coble, M. A., et al.
1029 (2016). Elucidating the magmatic history of the Austurhorn silicic intrusive complex
1030 (southeast Iceland) using zircon elemental and isotopic geochemistry and geochronology.
1031 *Contributions to Mineralogy and Petrology*, *171*(8), 69. https://doi.org/10.1007/s00410-
1032 016-1279-z
1033 Pálmason, G. (1986). Model of crustal formation in Iceland and application to submarine mid-

ocean ridges. In P. R. Vogt & B. E. Tucholke (Eds.), *The Geology of North America, vol. M, The Western North Atlantic Region* (pp. 87–98). Boulder, CO: Geological Society of America.

Peate, D. W., Breddam, K., Baker, J. A., Kurz, M. D., Barker, A. K., Prestvik, T., et al. (2010). Compositional Characteristics and Spatial Distribution of Enriched Icelandic Mantle Components. *Journal of Petrology*, *51*(7), 1447–1475. https://doi.org/10.1093/petrology/egq025

Pope, E. C., Bird, D. K., & Arnórsson, S. (2013). Evolution of low-^{18}O Icelandic crust. *Earth and Planetary Science Letters*, *374*, 47–59. https://doi.org/10.1016/j.epsl.2013.04.043

Prestvik, T. (1980). Petrology of hybrid intermediate and silicic rocks from Öræfajökull, southeast Iceland. *Geologiska Föreningen i Stockholm Förhandlingar*, *101*(4), 299–307. https://doi.org/10.1080/11035898009450848

Prestvik, T. (1982). Petrography, chemical characteristics and nomenclature of Öræfajökull rocks. *Jökull*, *32*, 69–76.

Prestvik, T., Goldberg, S., Karlsson, H., & Grönvold, K. (2001). Anomalous strontium and lead isotope signatures in the off-rift Öræfajökull central volcano in south-east Iceland: Evidence for enriched endmember(s) of the Iceland mantle plume? *Earth and Planetary Science Letters*, *190*(3–4), 211–220. https://doi.org/10.1016/S0012-821X(01)00390-9

Reid, M. R., Coath, C. D., Mark Harrison, T., & McKeegan, K. D. (1997). Prolonged residence times for the youngest rhyolites associated with Long Valley Caldera:^{230}Th—^{238}U ion microprobe dating of young zircons. *Earth and Planetary Science Letters*, *150*(1), 27–39. https://doi.org/10.1016/S0012-821X(97)00077-0

Reid, M. R., Vazquez, J. A., & Schmitt, A. K. (2011). Zircon-scale insights into the history of a

1057 Supervolcano, Bishop Tuff, Long Valley, California, with implications for the Ti-in-zircon
1058 geothermometer. *Contributions to Mineralogy and Petrology*, *161*(2), 293–311.
1059 https://doi.org/10.1007/s00410-010-0532-0
1060 Sæmundsson, K. (1979). Outline of geology of Iceland. *Jökull*, *29*, 7–28.
1061 Schärer, U. (1984). The effect of initial230Th disequilibrium on young U-Pb ages: the Makalu
1062 case, Himalaya. *Earth and Planetary Science Letters*, *67*(2), 191–204.
1063 https://doi.org/10.1016/0012-821X(84)90114-6
1064 Schattel, N., Portnyagin, M., Golowin, R., Hoernle, K., & Bindeman, I. (2014). Contrasting
1065 conditions of rift and off-rift silicic magma origin on Iceland. *Geophysical Research*
1066 *Letters*, *41*(16), 5813–5820. https://doi.org/10.1002/2014GL060780
1067 Schmitt, A. K., Grove, M., Harrison, T. M., Lovera, O., Hulen, J., & Walters, M. (2003). The
1068 Geysers - Cobb Mountain Magma System, California (Part 1): U-Pb zircon ages of volcanic
1069 rocks, conditions of zircon crystallization and magma residence times. *Geochimica et*
1070 *Cosmochimica Acta*, *67*(18), 3423–3442. https://doi.org/10.1016/S0016-7037(03)00140-6
1071 Sharp, Z. D. (1990). A laser-based microanalytical method for the in situ determination of
1072 oxygen isotope ratios of silicates and oxides. *Geochimica et Cosmochimica Acta*, *54*(5),
1073 1353–1357. https://doi.org/10.1016/0016-7037(90)90160-M
1074 Sigmarsson, O. (1996). Short magma chamber residence time at an Icelandic volcano inferred
1075 from U-series disequilibria. *Nature*, *382*(6590), 440–442. https://doi.org/10.1038/382440a0
1076 Sigmarsson, O., Hemond, C., Condomines, M., Fourcade, S., & Oskarsson, N. (1991). Origin of
1077 silicic magma in Iceland revealed by Th isotopes. *Geology*, *19*(6), 621–624.
1078 https://doi.org/10.1130/0091-7613(1991)019%3C0621:OOSMII%3E2.3.CO;2
1079 Sigmarsson, O., Condomines, M., & Fourcade, S. (1992a). A detailed Th, Sr and O isotope study

of Hekla: differentiation processes in an Icelandic volcano. *Contributions to Mineralogy and Petrology*, *112*, 20–34. https://doi.org/10.1007/BF00310953

Sigmarsson, O., Condomines, M., & Fourcade, S. (1992b). Mantle and crustal contribution in the genesis of Recent basalts from off-rift zones in Iceland: Constraints from Th, Sr and O isotopes. *Earth and Planetary Science Letters*, *110*(1–4), 149–162. https://doi.org/10.1016/0012-821X(92)90045-W

Simon, J. I., & Reid, M. R. (2005). The pace of rhyolite differentiation and storage in an 'archetypical' silicic magma system, Long Valley, California. *Earth and Planetary Science Letters*, *235*(1), 123–140. https://doi.org/10.1016/j.epsl.2005.03.013

Sláma, J., Kosler, J., Condon, D. J., Crowley, J. L., Gerdes, A., Hanchar, J. M., et al. (2008). Plešovice zircon-A new natural standard for U-Pb and Hf isotopic microanalysis. *Chemical Geology*, *249*(1–2), 1–35. https://doi.org/10.1016/j.chemgeo.2007.11.005

Spulber, S. D., & Rutherford, M. J. (1983). The Origin of Rhyolite and Plagiogranite in Oceanic Crust: An Experimental Study. *Journal of Petrology*, *24*(1), 1–25. https://doi.org/10.1093/petrology/24.1.1

Stacey, J. S., & Kramers, J. D. (1975). Approximation of terrestrial lead isotope evolution by a two-stage model. *Earth and Planetary Science Letters*, *26*(2), 207–221. https://doi.org/10.1016/0012-821X(75)90088-6

Stecher, O., Carlson, R. W., & Gunnarsson, B. (1999). Torfajökull: a radiogenic end-member of the Iceland Pb-isotopic array. *Earth and Planetary Science Letters*, *165*(1), 117–127. https://doi.org/10.1016/S0012-821X(98)00256-8

Stelten, M. E., & Cooper, K. M. (2012). Constraints on the nature of the subvolcanic reservoir at South Sister volcano, Oregon from U-series dating combined with sub-crystal trace-element

1103 analysis of plagioclase and zircon. *Earth and Planetary Science Letters*, *313–314*(1), 1–11.
1104 https://doi.org/10.1016/j.epsl.2011.10.035
1105 Storck, J.-C., Wotzlaw, J.-F., Karakas, Ö., Brack, P., Gerdes, A., & Ulmer, P. (2020). Hafnium
1106 isotopic record of mantle-crust interaction in an evolving continental magmatic system.
1107 *Earth and Planetary Science Letters*, *535*, 116100.
1108 https://doi.org/10.1016/j.epsl.2020.116100
1109 Thirlwall, M. F., Gee, M. A. M., Taylor, R. N., & Murton, B. J. (2004). Mantle components in
1110 Iceland and adjacent ridges investigated using double-spike Pb isotope ratios. *Geochimica*
1111 *et Cosmochimica Acta*, *68*(2), 361–386. https://doi.org/10.1016/S0016-7037(03)00424-1
1112 Thirlwall, M. F., Gee, M. A. M., Lowry, D., Mattey, D. P., Murton, B. J., & Taylor, R. N.
1113 (2004). Low $\delta^{18}O$ in the Icelandic mantle and its origins: Evidence from Reykjanes Ridge
1114 and Icelandic lavas. *Geochimica et Cosmochimica Acta*, *70*(4), 993–1019.
1115 https://doi.org/10.1016/j.gca.2005.09.008
1116 Thordarson, T., & Larsen, G. (2007). Volcanism in Iceland in historical time: Volcano types,
1117 eruption styles and eruptive history. *Journal of Geodynamics*, *43*(43), 118–152.
1118 https://doi.org/10.1016/j.jog.2006.09.005
1119 Thordarson, T., & Höskuldsson, Á. (2014). *Classic Geology in Europe 3: Iceland* (2nd ed.).
1120 Edinburgh: Dunedin Academic Press.
1121 Thy, P., Beard, J. S., & Lofgren, G. E. (1990). Experimental Constraints on the Origin of
1122 Icelandic Rhyolites. *The Journal of Geology*, *98*(3), 417–421.
1123 https://doi.org/10.1086/629413
1124 Torsvik, T. H., Amundsen, H. E. F., Tronnes, R. G., Doubrovine, P. V., Gaina, C., Kusznir, N. J.,
1125 et al. (2015). Continental crust beneath southeast Iceland. *Proceedings of the National*

1126 *Academy of Sciences*, E1818–E1827. https://doi.org/10.1073/pnas.1423099112
1127 Trail, D., Bindeman, I. N., Watson, E. B., & Schmitt, A. K. (2009). Experimental calibration of
1128 oxygen isotope fractionation between quartz and zircon. *Geochimica et Cosmochimica*
1129 *Acta*, *73*(23), 7110–7126. https://doi.org/10.1016/J.GCA.2009.08.024
1130 Valley, J. W., Lackey, J. S., Cavosie, A. J., Clechenko, C. C., Spicuzza, M. J., Basei, M. A. S., et
1131 al. (2005). 4.4 billion years of crustal maturation: oxygen isotope ratios of magmatic zircon.
1132 *Contributions to Mineralogy and Petrology*, *150*(6), 561–580.
1133 https://doi.org/10.1007/s00410-005-0025-8
1134 Valley, John W, Kinny, P. D., Schulze, D. J., & Spicuzza, M. J. (1998). Zircon megacrysts from
1135 kimberlite: oxygen isotope variability among mantle melts. *Contributions to Mineralogy*
1136 *and Petrology*, *133*(1–2), 1–11. https://doi.org/10.1007/s004100050432
1137 https://doi.org/10.1016/j.gca.2011.07.046
1138 Vervoort, Jeff D, & Blichert-Toft, J. (1999). Evolution of the depleted mantle: Hf isotope
1139 evidence from juvenile rocks through time. *Geochimica et Cosmochimica Acta*, *63*(3–4),
1140 533–556. https://doi.org/10.1016/S0016-7037(98)00274-9
1141 Vervoort, Jeffrey D. (2010). Hf analyses in zircon by LA-MC-ICPMS: promise and pitfalls.
1142 *Geological Society of America Abstracts with Programs*, *42*, 286-289 (Abstract).
1143 Walker, George P L. (1964). Geological investigations in eastern Iceland. *Bulletin of*
1144 *Volcanology*, *27*(1), 351–363. https://doi.org/10.1007/BF02597532
1145 Walker, George P L. (1974). The structure of eastern Iceland. In *Geodynamics of Iceland and the*
1146 *North Atlantic Area* (pp. 177–188). Springer.
1147 Walker, George Patrick Leonard. (1966). Acid rocks in Iceland. *Bulletin of Volcanology*, *29*,
1148 375–402. https://doi.org/10.1007/BF02597164

1149 Walker, George Patrick Leonard. (1975). Excess spreading axes and spreading rate in Iceland.
1150 *Nature*, *255*(5508), 468–471. https://doi.org/10.1038/255468a0
1151 Walters, R. L., Jones, S. M., & Maclennan, J. (2013). Renewed melting at the abandoned
1152 Húnafloí Rift, northern Iceland, caused by plume pulsing. *Earth and Planetary Science*
1153 *Letters*, *377*, 227–238. https://doi.org/10.1016/j.epsl.2013.06.040
1154 Watson, E. B., Wark, D. A., & Thomas, J. B. (2006). Crystallization thermometers for zircon and
1155 rutile. *Contributions to Mineralogy and Petrology*, *151*(4), 413–433.
1156 https://doi.org/10.1007/s00410-006-0068-5
1157 Zellmer, G. F., Annen, C., Charlier, B. L. A., George, R. M. M., Turner, S. P., & Hawkesworth,
1158 C. J. (2005). Magma evolution and ascent at volcanic arcs: constraining petrogenetic
1159 processes through rates and chronologies. *Journal of Volcanology and Geothermal*
1160 *Research*, *140*(1), 171–191. https://doi.org/10.1016/j.jvolgeores.2004.07.020
1161 Zellmer, G. F., Rubin, K. H., Grönvold, K., & Jurado-Chichay, Z. (2008). On the recent bimodal
1162 magmatic processes and their rates in the Torfajökull–Veidivötn area, Iceland. *Earth and*
1163 *Planetary Science Letters*, *269*(3), 388–398.
1164 https://doi.org/https://doi.org/10.1016/j.epsl.2008.02.026

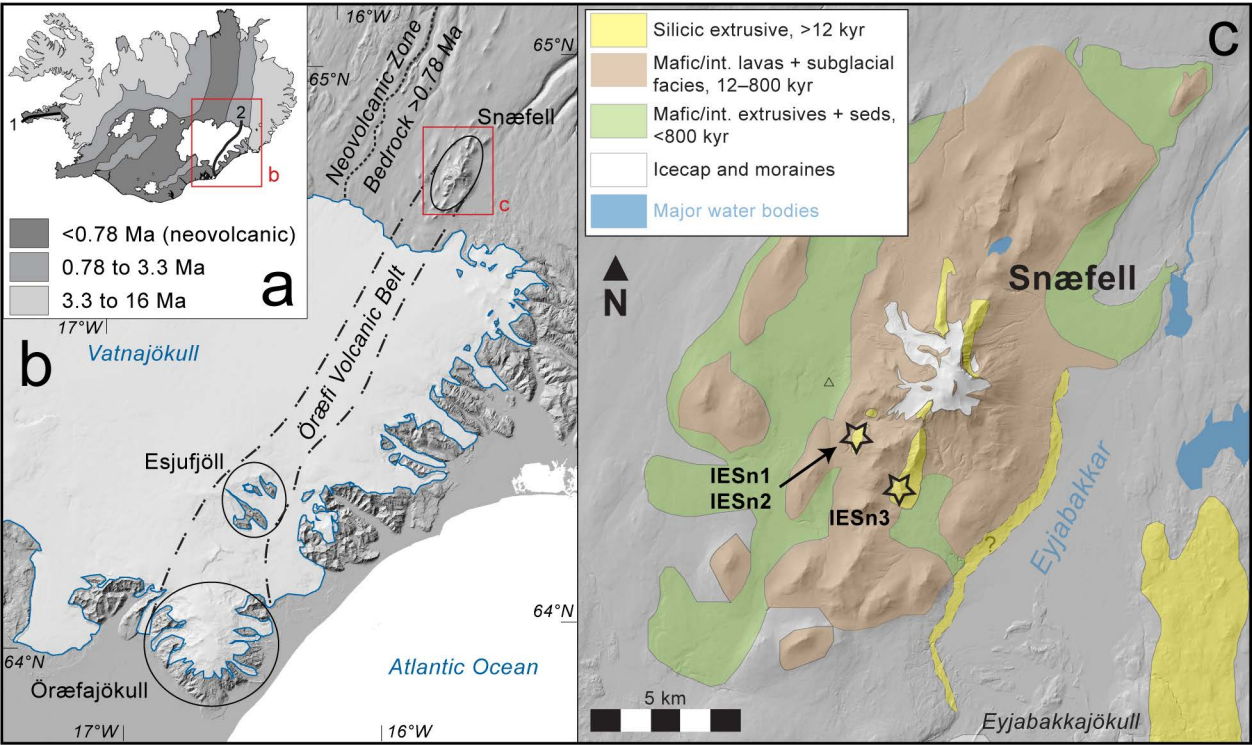
a
<0.78 Ma (neovolcanic)
0.78 to 3.3 Ma
3.3 to 16 Ma
1
2
b
b
16°W
65°N
17°W
Vatnajökull
Neovolcanic Zone
Bedrock >0.78 Ma
Snæfell
c
Öræfi Volcanic Belt
Esjufjöll
64°N
Öræfajökull
Atlantic Ocean
C
Silicic extrusive, >12 kyr
Mafic/int. lavas + subglacial facies, 12–800 kyr
Mafic/int. extrusives + seds, <800 kyr
Icecap and moraines
Major water bodies
N
Snæfell
IESn1
IESn2
IESn3
Eyjabakkar
?
5 km
Eyjabakkajökull

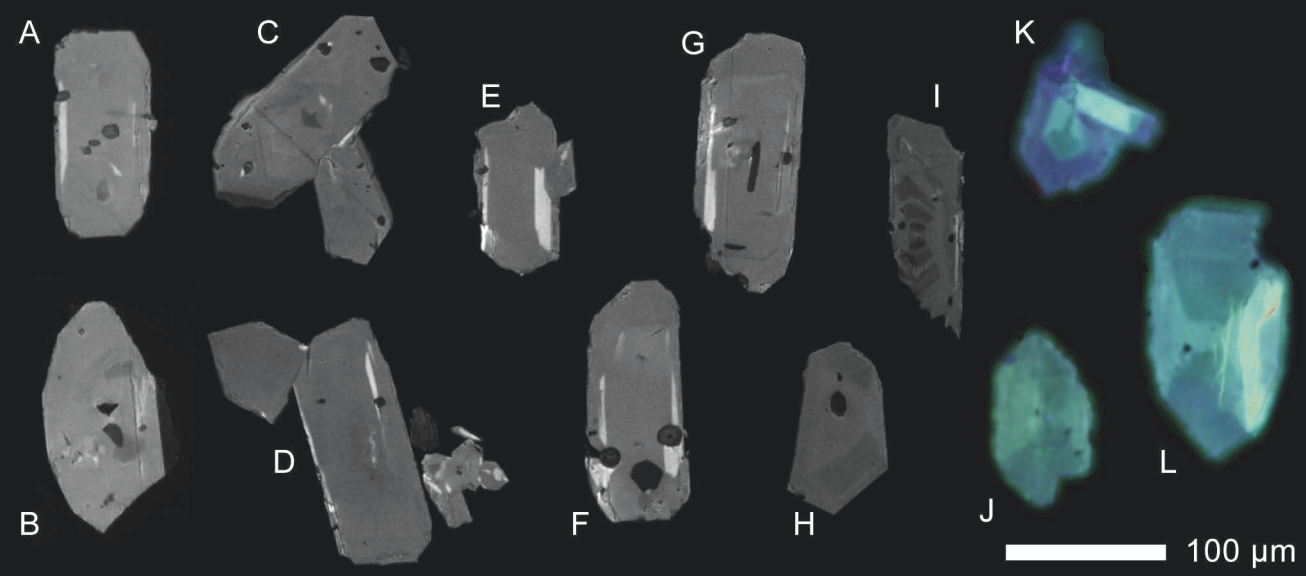
A
C
E
G
I
K
B
D
F
H
J
L
100 µm

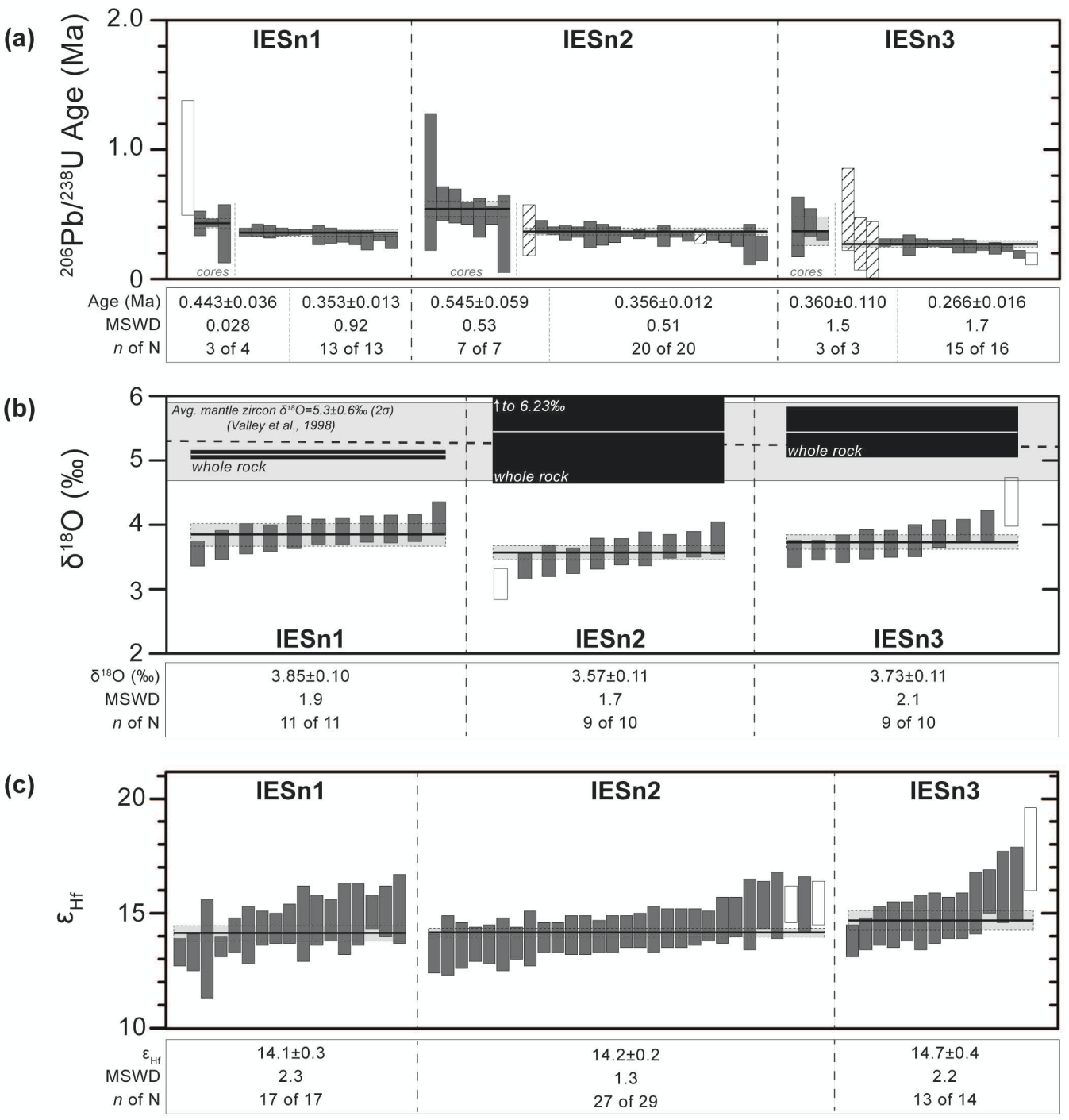
(a)
IESn1
IESn2
IESn3
$^{206}Pb/^{238}U$ Age (Ma)
2.0
1.0
0
cores
cores
cores
Age (Ma) 0.443±0.036 0.353±0.013 0.545±0.059 0.356±0.012 0.360±0.110 0.266±0.016
MSWD 0.028 0.92 0.53 0.51 1.5 1.7
n of N 3 of 4 13 of 13 7 of 7 20 of 20 3 of 3 15 of 16
(b)
Avg. mantle zircon δ18O=5.3±0.6‰ (2σ)
(Valley et al., 1998)
whole rock
↑ to 6.23‰
whole rock
whole rock
δ18O (‰)
6
5
4
3
2
IESn1
IESn2
IESn3
δ18O (‰) 3.85±0.10 3.57±0.11 3.73±0.11
MSWD 1.9 1.7 2.1
n of N 11 of 11 9 of 10 9 of 10
(c)
IESn1
IESn2
IESn3
εHf
20
15
10
εHf 14.1±0.3 14.2±0.2 14.7±0.4
MSWD 2.3 1.3 2.2
n of N 17 of 17 27 of 29 13 of 14

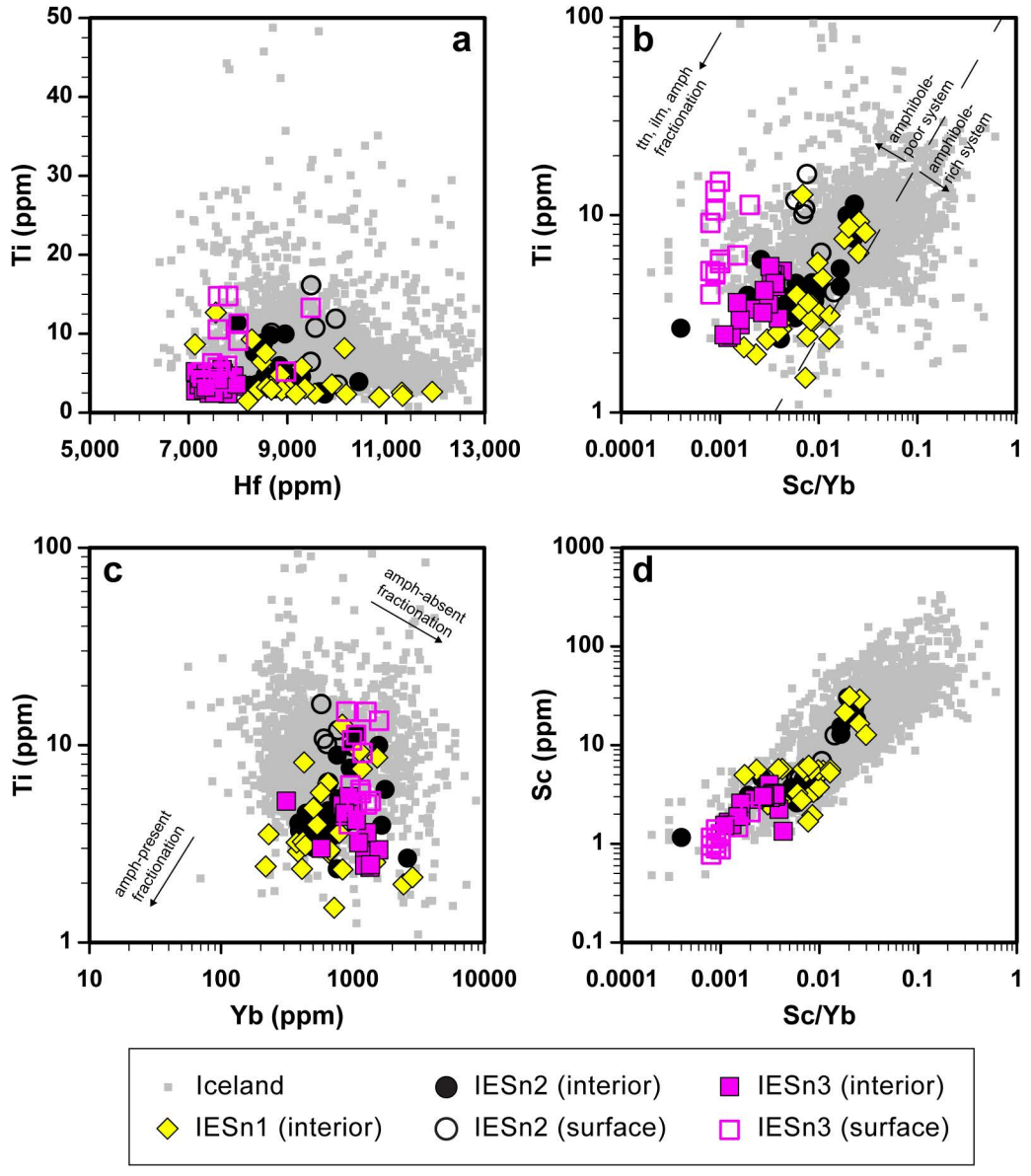
a
Ti (ppm)
Hf (ppm)
b
ttn, ilm, amph fractionation
amphibole-poor system
amphibole-rich system
Ti (ppm)
Sc/Yb
c
amph-absent fractionation
amph-present fractionation
Ti (ppm)
Yb (ppm)
d
Sc (ppm)
Sc/Yb
Iceland
IESn1 (interior)
IESn2 (interior)
IESn2 (surface)
IESn3 (interior)
IESn3 (surface)

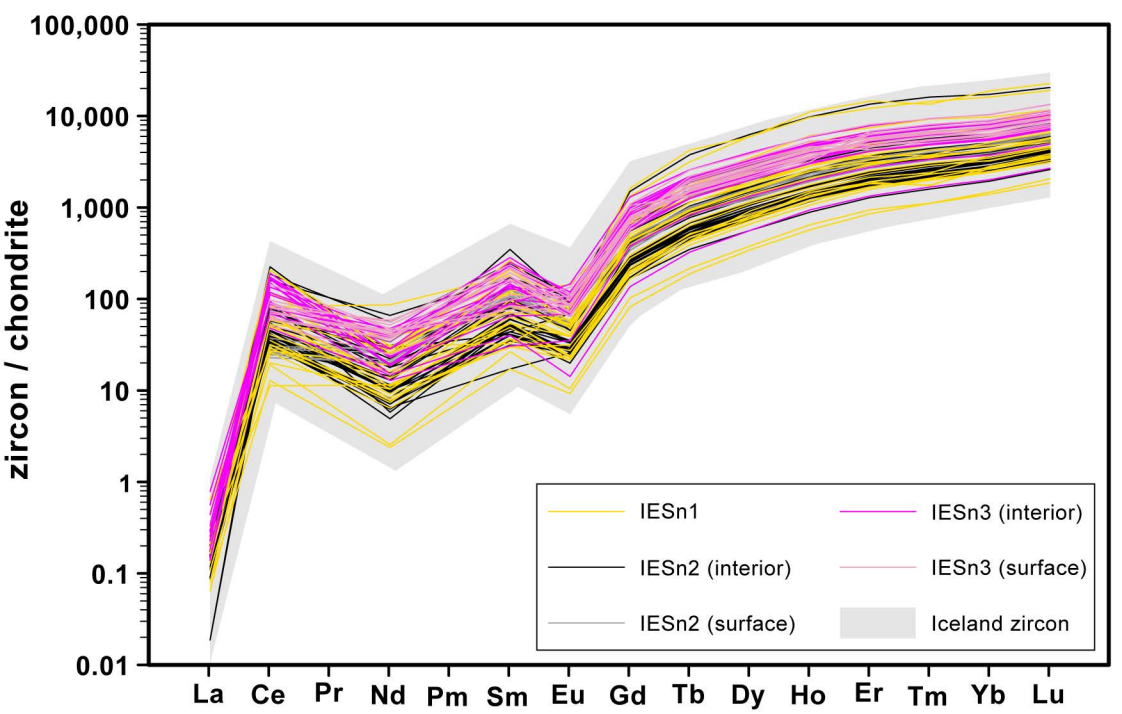
100,000
10,000
1,000
100
10
1
0.1
0.01
zircon / chondrite
La
Ce
Pr
Nd
Pm
Sm
Eu
Gd
Tb
Dy
Ho
Er
Tm
Yb
Lu
IESn1
IESn2 (interior)
IESn2 (surface)
IESn3 (interior)
IESn3 (surface)
Iceland zircon

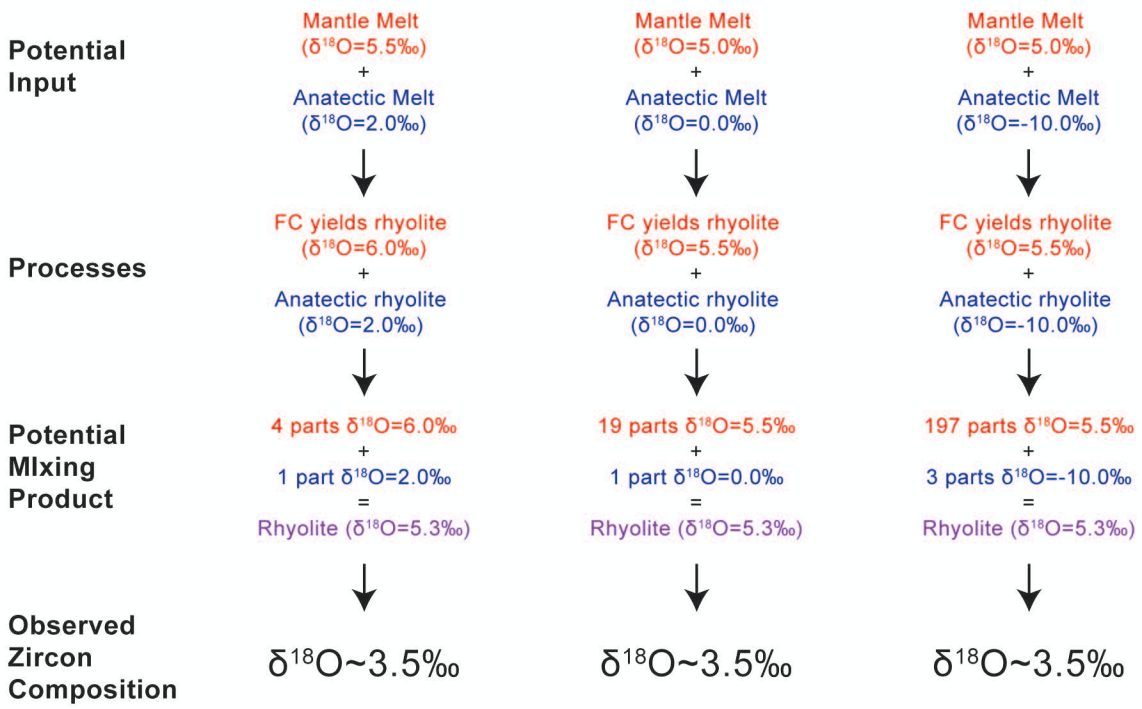
Potential Input
Processes
Potential MIxing Product
Observed Zircon Composition
Mantle Melt (δ18O=5.5‰)
+
Anatectic Melt (δ18O=2.0‰)
FC yields rhyolite (δ18O=6.0‰)
+
Anatectic rhyolite (δ18O=2.0‰)
4 parts δ18O=6.0‰
+
1 part δ18O=2.0‰
=
Rhyolite (δ18O=5.3‰)
δ18O~3.5‰
Mantle Melt (δ18O=5.0‰)
+
Anatectic Melt (δ18O=0.0‰)
FC yields rhyolite (δ18O=5.5‰)
+
Anatectic rhyolite (δ18O=0.0‰)
19 parts δ18O=5.5‰
+
1 part δ18O=0.0‰
=
Rhyolite (δ18O=5.3‰)
δ18O~3.5‰
Mantle Melt (δ18O=5.0‰)
+
Anatectic Melt (δ18O=-10.0‰)
FC yields rhyolite (δ18O=5.5‰)
+
Anatectic rhyolite (δ18O=-10.0‰)
197 parts δ18O=5.5‰
+
3 parts δ18O=-10.0‰
=
Rhyolite (δ18O=5.3‰)
δ18O~3.5‰

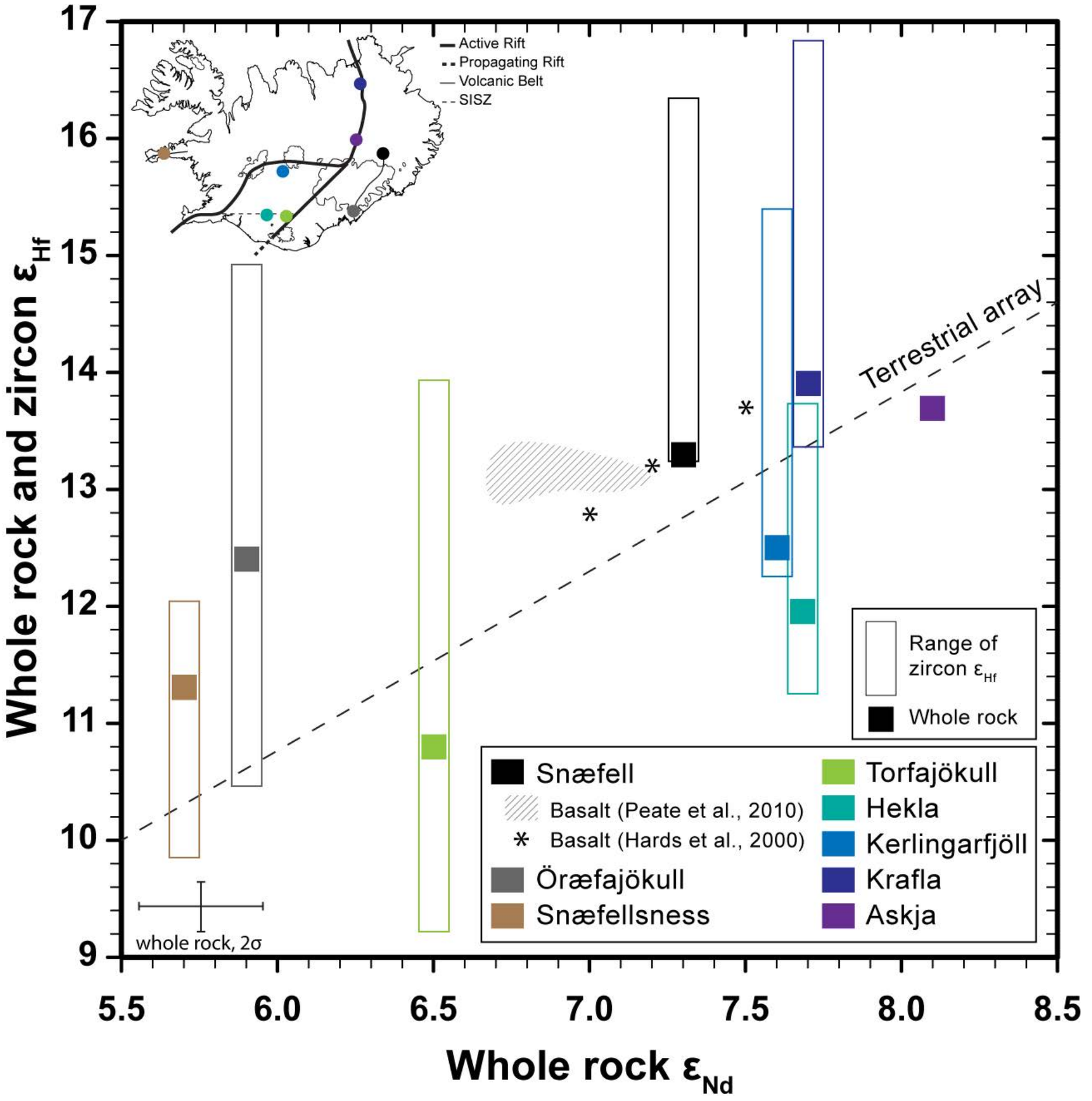
Active Rift
Propagating Rift
Volcanic Belt
SISZ
Terrestrial array
Range of zircon ε_{Hf}
Whole rock
Snæfell
Basalt (Peate et al., 2010)
Basalt (Hards et al., 2000)
Öræfajökull
Snæfellsness
Torfajökull
Hekla
Kerlingarfjöll
Krafla
Askja
whole rock, 2σ
Whole rock and zircon ε_{Hf}
Whole rock ε_{Nd}
17
16
15
14
13
12
11
10
9
5.5
6.0
6.5
7.0
7.5
8.0
8.5

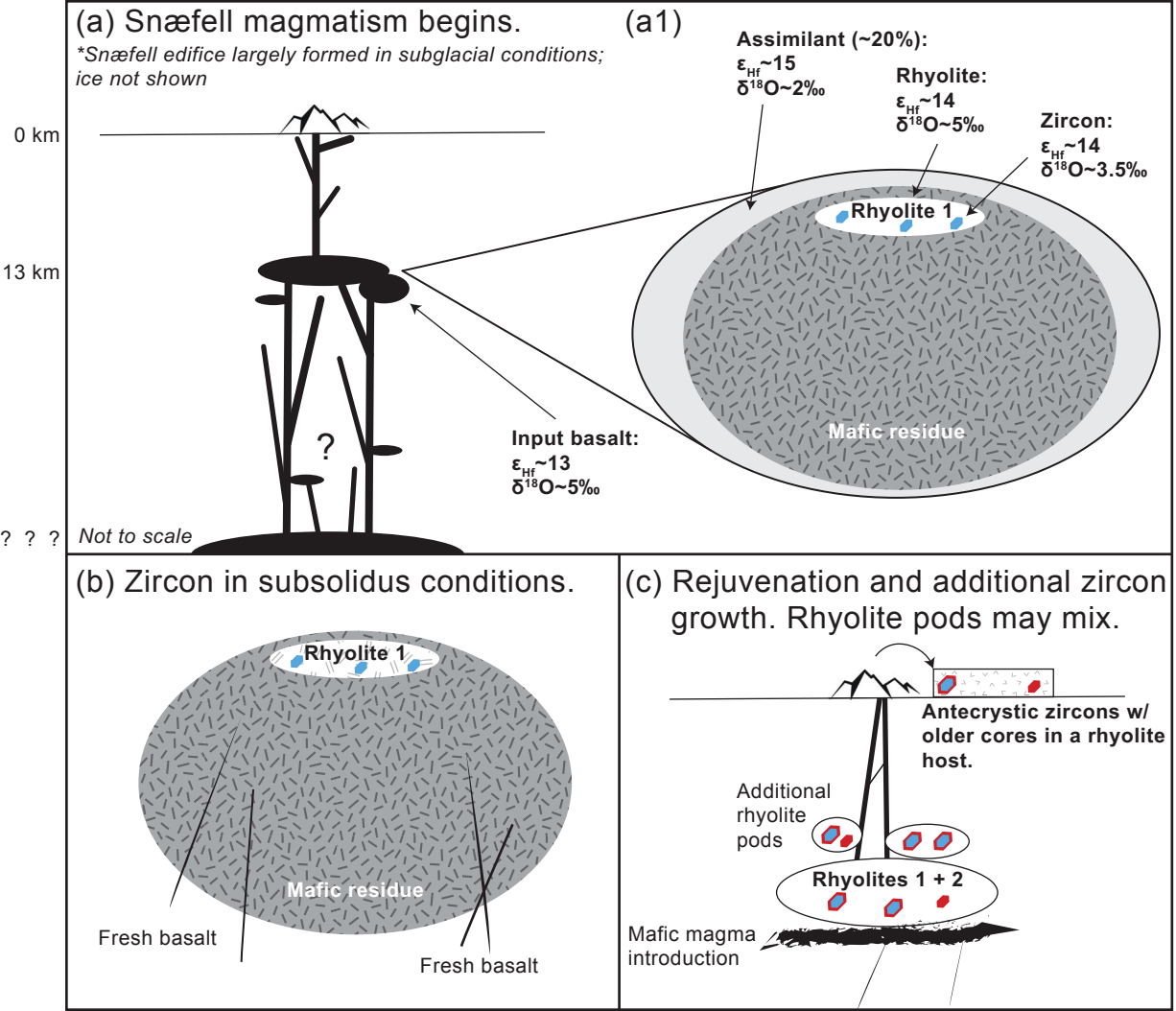
(a) Snæfell magmatism begins.
*Snæfell edifice largely formed in subglacial conditions; ice not shown
(a1)
Assimilant (~20%):
ε_{Hf}~15
$\delta^{18}O$~2‰
Rhyolite:
ε_{Hf}~14
$\delta^{18}O$~5‰
Zircon:
ε_{Hf}~14
$\delta^{18}O$~3.5‰
Rhyolite 1
Mafic residue
Input basalt:
ε_{Hf}~13
$\delta^{18}O$~5‰
0 km
13 km
?
? ? ?
Not to scale
(b) Zircon in subsolidus conditions.
Rhyolite 1
Mafic residue
Fresh basalt
Fresh basalt
(c) Rejuvenation and additional zircon growth. Rhyolite pods may mix.
Antecrystic zircons w/ older cores in a rhyolite host.
Additional rhyolite pods
Rhyolites 1 + 2
Mafic magma introduction

Supplementary Figure S1. Zircon images and analytical spots. All images are cathodoluminescence except when specified otherwise.

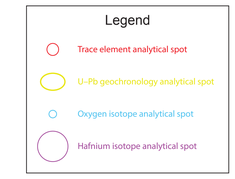

Sample: IESn1 (*aka* Sn1) **Mount:** TJB.15

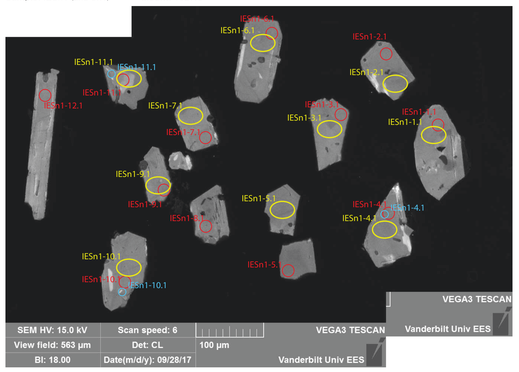

Sample: IESn1 (*aka* Sn1) **Mount:** TJB.16

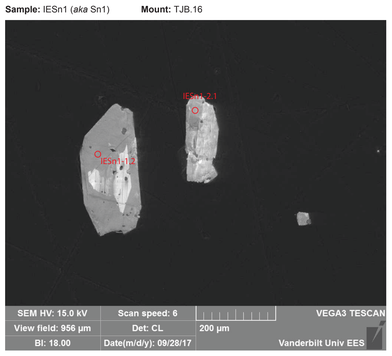

Sample: IESn1 (*aka* Sn1) **Mount:** TJB.18

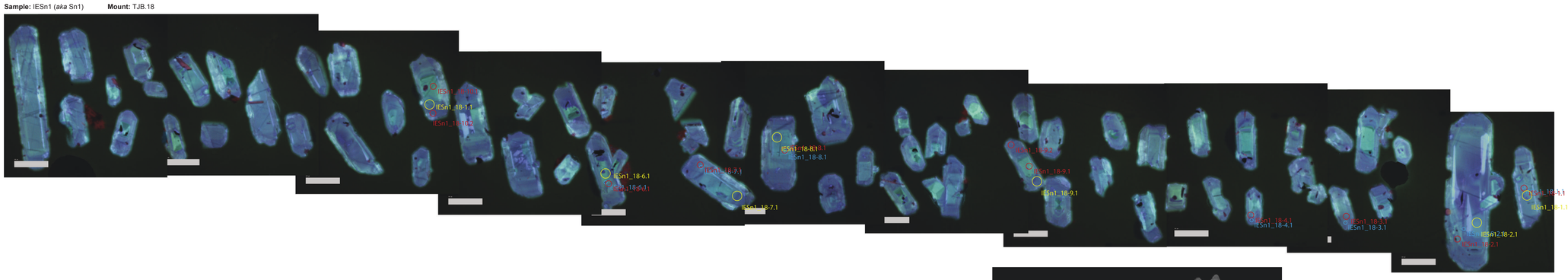

Sample: IESn2 (*aka* Sn2) **Mount:** TJB.15

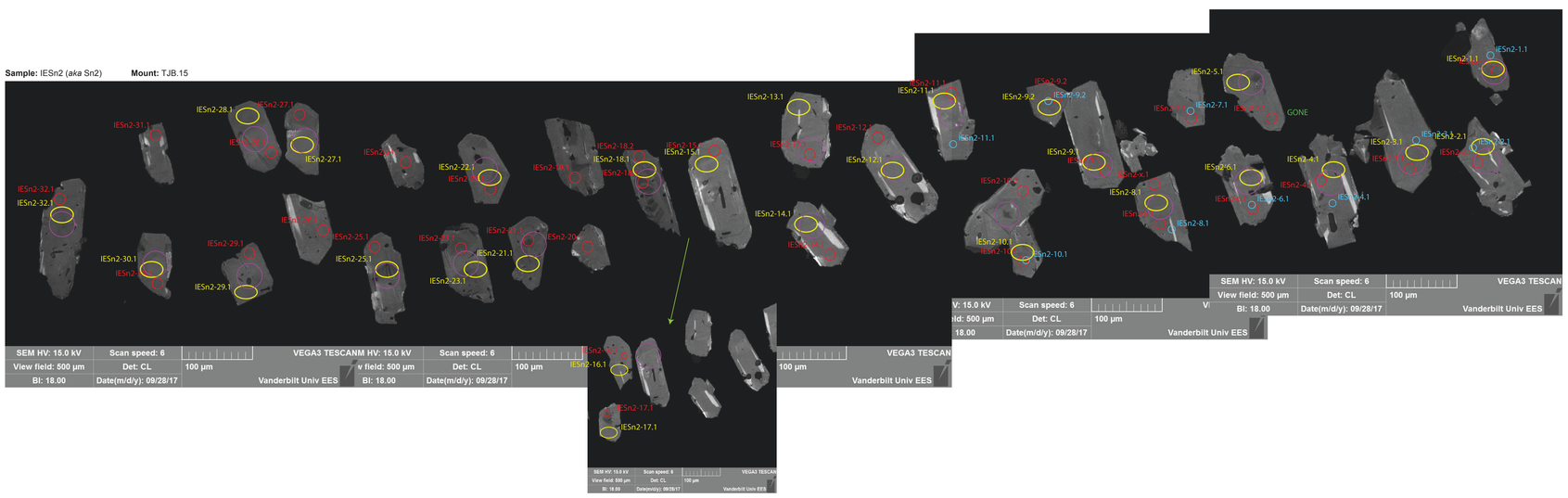

Sample: IESn2 (*aka* Sn2) **Mount:** TJB.16

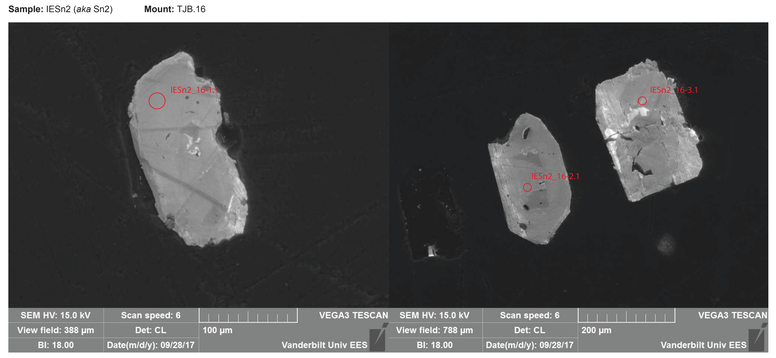

Sample: IESn2 (*aka* Sn2) **Mount:** TJB.17 **Image Type:** Reflected light

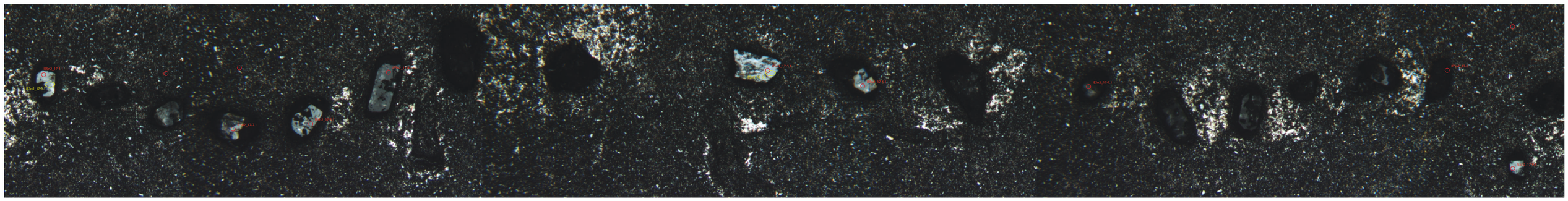

Sample: IESn3 (*aka* Sn3) **Mount:** TJB.15

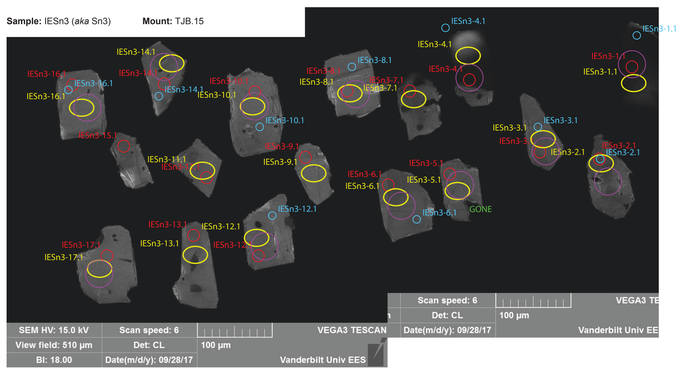

Sample: IESn3 (*aka* Sn3) **Mount:** TJB.16

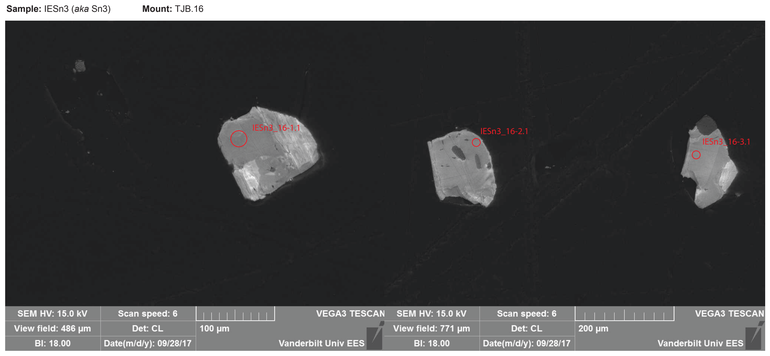

Sample: IESn3 (*aka* Sn3) **Mount:** TJB.17 **Image Type:** Reflected light